IEEE Access
Multidisciplinary ⋮ Rapid Review ⋮ Open Access Journal

Received 25 June 2025, accepted 17 July 2025, date of publication 22 July 2025, date of current version 31 July 2025.

Digital Object Identifier 10.1109/ACCESS.2025.3591485

RESEARCH ARTICLE

Novel Passivity Analysis for Wind Turbine Systems via Decentralized Event-Triggered Approach

R. VADIVEL[1], T. K. SANTHOSH[2], R. SURESH[3], NALLAPPAN GUNASEKARAN[4], MOHAMMED H. ALSHARIF[5], AND MUN-KYEOM KIM[6]

[1]Department of Mathematics, Faculty of Science and Technology, Phuket Rajabhat University, Phuket 83000, Thailand
[2]School of Electrical and Electronics Engineering, SASTRA Deemed University, Thanjavur 613401, India
[3]Department of Mathematics, Sri Venkateswara College of Engineering, Sriperumbudur, Tamil Nadu 602117, India
[4]Eastern Michigan Joint College of Engineering, Beibu Gulf University, Qinzhou 535011, China
[5]Department of AI Convergence Electronic Engineering, Sejong University, Seoul 05006, South Korea
[6]School of Energy System Engineering, Chung-Ang University, Dongjak-gu, Seoul 06974, Republic of Korea

Corresponding authors: R. Vadivel (vadivelsr@yahoo.com) and Mun-Kyeom Kim (mkim@cau.ac.kr)

This work was supported in part by Chung-Ang University Research Grants in 2025 under Grant CAU-2025, and in part by the National Research Foundation of Korea (NRF) grant funded by Korean Government under Grant RS-2025-16064833.

ABSTRACT This paper focuses on an innovative passivity analysis of wind turbine systems employing a decentralized event-triggered control approach. To establish new stability conditions, a novel Lyapunov-Krasovskii functional (LKF) is introduced, incorporating information from both the upper and lower bounds of the interval time-varying delay. We provide a new approach to identify the time instants of transmission from the sensors to the controller using just locally available information in event-triggered communication schemes. By using the relaxed integral inequality and the delay decomposition methodology, novel delay-dependent criteria guarantee that the considered system is passive. The passification problem is then handled by designing a decentralized event-triggered controller based on the acquired passivity conditions. The established stability conditions are expressed as linear matrix inequalities (LMIs), which may be numerically verified using the MATLAB LMI toolkit. Finally, a numerical example clearly demonstrates the superiority of our theoretical results using the simulation model.

INDEX TERMS Lyapunov-Krasovskii functional, passivity, delay decomposition approach, event-triggered control.

I. INTRODUCTION

Nowadays, population increase and economic development indicate a high energy demand, necessitating the development of novel electrical power plants to meet the growing global energy needs. These breakthroughs fueled tremendous technological breakthroughs in the direction of renewable energy sources (RESs), which began to gain traction. Because of their availability and considerably lower installation costs, wind, and solar energy are the most appealing renewable energy options for producing electrical power [1], [2]. Wind energy is widely considered one of the most viable and fastest-growing sources of renewable energy [3], [4]. Although other types of wind energy conversion systems (WECS) were presented in the literature, one of the most favorable systems in wind production systems is direct-drive WECS with a permanent magnet synchronous generator (PMSG). The primary benefit of employing a PMSG in place of a doubly fed induction generator in WECS is the comprehensive advantages, together with no DC excitation, minimal maintenance, and a high power-to-weight ratio [5], [6]. Furthermore, the wind turbine system can operate in fixed-speed or variable-speed modes. The variable-speed mode is recommended for the study due to its enhanced efficiency in WECS. Uncertain parameters and nonlinear properties are unavoidable when using the PMSG model.

The associate editor coordinating the review of this manuscript and approving it for publication was Mouquan Shen.

It should be mentioned that significant efforts have been made to investigate PMSG. The investigation of the stability performance of PMSG has recently become a popular subject of study within the research community [5], [7], [8], [9].

Time delays are a primary cause of instability and loss of attention in electrical energy systems, and they are also present in PMSGs due to feedback measurement lags. These time delays can significantly affect output power, voltage quality, system stability, and even lead to blackouts. The stability and stabilization analysis of differential systems in the context of WECS has been extensively studied in [10]. To achieve our objective of investigating PMSG stabilization, we need to develop a time-delay model that incorporates control strategies and uncertain parameters, while also considering stability performance. This is a challenging task, as we must balance all these factors to create an accurate and useful model. Because the PMSG with delays that change over time can affect how well the control works and even how stable the system is, they have been frequently addressed in the literature. Researchers have recently become interested in the PMSG model, as seen in [5], [9], [11], and [12]. Researchers feel that the presence of a time delay is the primary source of instability and performance degradation, which makes evaluating systems in control theory difficult. As a result, the LKF approach has been developed to successfully handle this problem [13], [14]. In [15], decentralized memory-based sampled-data control (SDC) was used to study the stability of delayed T-S fuzzy interconnected systems. Recently, in [16], authors studied the quantized dissipative control for wind production systems using the T-S fuzzy model.

The passivity theory was first suggested in circuit analysis (Bevelevich, 1968) and has brought numerous incredible examination interests, because of its uses in diverse exploration fields like stability, processing of signals, control of chaotic systems, fuzzy control, management of power systems, regulation of flow, etc ([17], [18]). Even while research on passivity has received a great deal of consideration, very little of it has been applied to the WECS passivity aspects. The passive system, in particular, uses the product of input and output as the energy provision and incorporates the energy attenuation property. In this way, the passivity analysis can be applied to the WECS. Passivity issues have been generally concentrated in [19], [20] (see Tables 1 and 2). Nevertheless, it ought to be noted that there are not many results that have been introduced on the passivity issues for WECS.

Advanced control mechanisms, including impulsive control, dissipative control, finite-time control, dependable control, and sampled-data control, have been extensively investigated for the stabilization of unstable and networked systems [9], [16], and [21]. Based on the above-mentioned control, Event-triggered control (ETC) has emerged as a prominent approach for improving efficiency in networked environments by updating control actions solely when required, thus reducing communication loads relative to periodic strategies [22], [23], [24], and [25]. Centralized ETC facilitates globally coordinated decisions; however, it is hindered by scalability and communication bottlenecks [26], [27]. Periodic ETC diminishes data transmissions to a degree but continues to depend on fixed-time sampling [28]. Additionally, hybrid schemes that integrate time and event-based updates frequently necessitate synchronization among subsystems. The proposed decentralized event-triggered control (DETC) framework allows each wind turbine to independently assess its local triggering condition based solely on local information, thereby eliminating the need for continuous communication and central coordination. This decentralized architecture improves scalability, resilience to delays, and energy efficiency, particularly in extensive, spatially distributed wind farms [24], [29], and [30]. The proposed DETC scheme integrates a passivity-based design, ensuring global energy-based stability under asynchronous and sparse updates, thus providing a theoretically robust and practically efficient control solution for wind turbine systems. In this manner, the DETC innovation has demonstrated an increasing predominance over other control approaches. Despite the fact that the relevance of DETC management and passivity features has been widely recognized, the event-triggered challenges of passivity and passification for the PMSG model have yet to be addressed and remain unresolved. The structure of the proposed control scheme has been represented in Figure 1.

Inspired by the aforementioned discussions, this article is concerned with the Passivity analysis for the PMSG model with delay decomposition approach (DDA) via event-triggered control. In particular, compared to the previous PMSG models, the novelty of this general time delay lies in its modeled system, and the uncertain parameter parts are considered comprehensively. Hence, the foremost innovations and salient contributions of this article over the relevant reports are concretely reflected in the following points:

1) Based on the passivity and passification theory, the problem of DETC of PMSG is investigated.

2) The chosen Lyapunov-Krasovskii functional (LKF) is enhanced with more input delay-dependent information using the DDA and DETC technique.

3) The DETC technique is utilized to optimize the limited network resources in conjunction with the PMSG model.

4) By constructing an appropriate Lyapunov-Krasovskii functional together with relaxed integral inequality and other inequality approaches, novel passivity criteria are established in the form of linear matrix inequalities. 5) Finally, numerical examples with simulation results are included at the end of this study to demonstrate the efficacy of the DETC mechanism described in this study.

Notation: The notation $\mathcal{X} \in \mathbb{R}^{n\times m}$ means that $\mathcal{X}$ is an $n \times m$ matrix with real entries. $\mathcal{X} > 0$ or $\mathcal{X} \geq 0$, it means that $\mathcal{X}$ is positive definite or positive semi-definite,

TABLE 1. Comparison of key features in wind turbine models.

Aspect	[5]	[8]	[9]	[12]	[16]	Our paper
DETC	✗	✗	✗	✗	✗	✓
Passivity Analysis	✗	✗	✗	✗	✗	✓
Delay Consideration in WEC	✗	✗	✗	✓	✓	✓
Uncertainty (ΔA, ΔB)	✓	✗	✓	✓	✓	✓
Non-fragile -Controller Design	✗	✗	✓	✗	✗	✓
DDA-LKF	✗	✗	✗	✗	✗	✓

TABLE 2. Summary of relevant research works.

Reference	Main contribution	Relevance to current Work
[2]	Studied a direct-driven PMSG wind turbine for the power system.	Addresses decentralized event-triggered control of the PMSG wind turbines.
[4]	Investigated memory-based integral SMC for nonlinear DFIG-based wind turbines using T-S fuzzy.	Focuses on PMSG wind turbine using DETC, whereas our work emphasizes both uncertainties and passivity behaviour.
[18]	Studied delay-dependent passivity conditions for NNs with time-varying delays and uncertainties.	Provides theoretical insights into DDA handling, which supports our LKF-based approach for the proposed model with DETC.
[21]	Studied robust event-triggered control for T-S fuzzy systems with uncertainties, using weighted inequalities to ensure reliability and stability.	Our work focuses on the DETC and robust passivity analysis for the PMSG wind turbines.
[30]	Investigated communication schemes for centralized and decentralized event-triggered control, optimizing resource usage in networked systems.	While our work does not focus on the centralized, it incorporates decentralized ETC in the presence of uncertainty to improve efficiency.
[31]	Developed a Passivity-based fuzzy ISMC for wind energy conversion systems with PMSG.	Highlights and enhance the effects of variation of wind speed and reference voltage in the PMSG wind turbines using OPAL-RT.

respectively. The inverse and transpose of a matrix Q are denoted by Q^{-1} and Q^T, respectively. The identity matrix with the corresponding dimensions is denoted by I. When dealing with symmetric matrices, we use the notation $*$ to indicate the symmetric terms. The notation $\mathbb{R}^n$ represents the n-dimensional Euclidean space, while $\mathbb{R}^{n\times m}$ represents the set of $n \times m$ real matrices. Finally, if we have a set I_{17} with 17 elements, then for any $\bar{j}$ in that set, we can denote the block entry matrix $a_{\bar{j}}$ as $[0_{n\times(\bar{j}-1)n} \quad I \quad 0n \times (17-\bar{j})n]$. Moreover, $\forall\ \bar{j} \in I_{17}$, we denote the block entry matrices $a_{\bar{j}} = [0_{n\times(\bar{j}-1)_n} \quad I \quad 0_{n\times(17-\bar{j})n}]$, $\bar{j} = 1, 2, \cdots, 17$, for example: $a_5 = [\underbrace{0\ldots0}_{4\ times} \ I \ \underbrace{0\ldots0}_{12\ times}]$.

II. PROBLEM FORMULATION AND PRELIMINARIES

Consider a wind with an air mass $\hat{m}$, pressure $\hat{p}$, density $\hat{\rho}$, and velocity $\hat{v}$ imparts momentum $\hat{H} = \hat{m}(\hat{v}_u - \hat{v}_w)$ onto a disk with a cross-sectional area $\hat{A}$. Then, the resultant force is:

$$\hat{F} = \frac{\Delta\hat{H}}{\Delta t} = \frac{\Delta\hat{m}(\hat{v}_u - \hat{v}_w)}{\Delta t} = \hat{\rho}\hat{A}\hat{v}_0(\hat{v}_u - \hat{v}_w). \tag{1}$$

Moreover, the wind force is stated as,

$$\hat{F} = \frac{1}{2}\hat{\rho}\hat{A}(\hat{v}_u^2 - \hat{v}_w^2). \tag{2}$$

Using (1)-(2), the wind speed at the actuator disk may be calculated with the input and output wind speed as $\hat{v}_0 = \frac{1}{2}(\hat{v}_u + \hat{v}_w)$. The power coefficient $C_{\hat{p}}$ is defined as

$$C_{\hat{p}} = \frac{\hat{P}_{wt}}{\hat{P}_{wind}} = 4\hat{a}(1-\hat{a})^{\cdot} \tag{3}$$

From (3), $C_{\hat{p}}$ reaches its highest value $C_{\hat{p},max} = 0.59$ at $\hat{a} = 1/3$ (referred to as the Betz limit), which represents the WECS's maximum power extraction in the ideal condition.

Performance of Non-Ideal Wind Turbine. As illustrated in Figure 2, the greatest possible power extraction for the majority of WECS is roughly 70% to 80% of the Betz

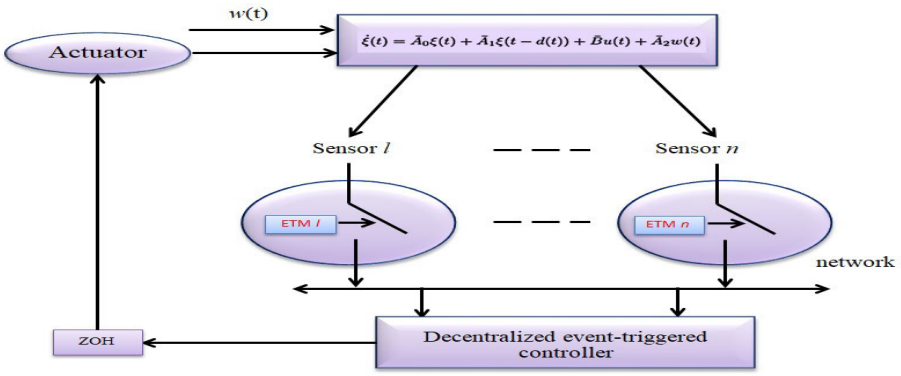

FIGURE 1. Structure of the proposed control scheme.

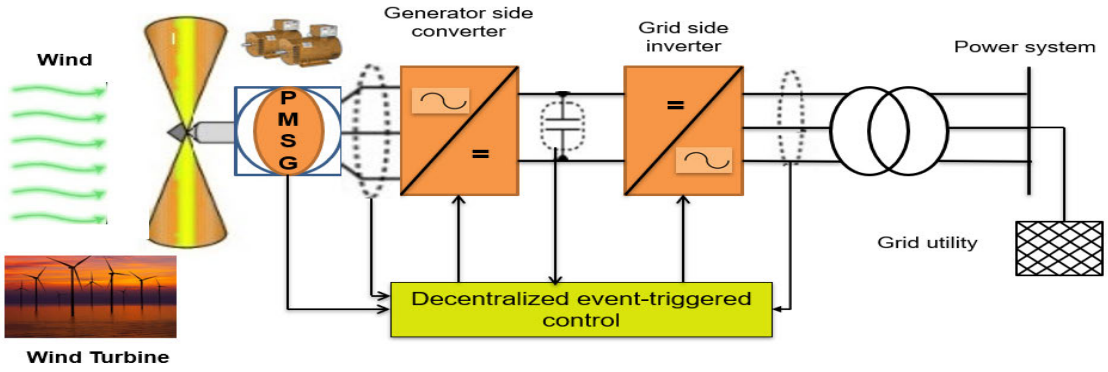

FIGURE 2. Schematic diagram for PMSG-WECS.

limit. Hence $C_{\hat{p}} = \frac{\hat{P}_{wt}}{\hat{P}_{wind}} < 0.5$. Here, $\hat{\lambda}$ is defined as the relationship between the speed of the outer blades and the corresponding wind speed $\hat{v}$,

$$\hat{\lambda} = \frac{\omega_r \hat{R}_t}{\hat{v}}, \tag{4}$$

where $\hat{R}_t$ denotes the turbine blade length and ω_r denotes the mechanical rotational speed of the rotor.

Assuming a wind turbine with blade pitch angle $\hat{\beta} = 0^o$, the constants $\hat{c}_1$ to $\hat{c}_7$ are given as $\hat{c}_1 = 0.39, \hat{c}_2 = 116, \hat{c}_3 = 0.4, \hat{c}_4 = 5, \hat{c}_5 = 16.5, \hat{c}_6 = 0.089$, and $\hat{c}7 = 0.035$. Using these constants, the maximum power coefficient is calculated to be $C\hat{p}, max = 0.4953$, which is a typical value for wind turbines. Additionally, the optimum tip speed ratio is calculated to be $\hat{\lambda}_o = 7.2$, which is also within the expected range for wind turbines.

The wind turbine's aerodynamic torque is calculated as follows:

$$\tau_{\hat{m}} = \frac{\hat{P}_{wt}}{\omega_r} = \frac{1}{2}\frac{\hat{\rho} C_{\hat{p}} \pi \hat{R}_t^2 \hat{v}^3}{\omega_r}. \tag{5}$$

Therefore, from (5) becomes

$$\tau_{\hat{m}} = \frac{\hat{\rho}\pi \hat{R}_t^3 C_{\hat{p}}(\hat{\lambda}, \hat{\beta})\hat{v}^2}{2\hat{\lambda}} = \frac{1}{2\omega_r}\hat{\rho}\hat{A}\hat{v}^3 C_{\hat{p}}(\hat{\lambda}, \hat{\beta}). \tag{6}$$

The torque coefficient $C_{\hat{q}}$ describes the rotor output torque and is useful for evaluating the performance of a wind turbine. For example, given the optimum tip speed ratio $\hat{\lambda}o$, the maximum torque coefficient $C\hat{q}, max$ can be obtained. The above equation (6) is used to calculate the mechanical torque obtained from the wind. It takes into account the density of the air ($\hat{\rho}$), the radius of the rotor blades ($\hat{R}$), the wind speed ($\hat{v}$), and the torque coefficient ($C_{\hat{q}}$), which depends on the tip speed ratio ($\hat{\lambda}$) and the pitch angle ($\hat{\beta}$). The torque coefficient is obtained by dividing the power coefficient by the tip speed ratio, as mentioned earlier. The resulting mechanical torque is an important parameter for evaluating the performance of a wind turbine system and for controlling its operation.

PMSG Model: Consider the following direct and quadrature axis voltage of the PMSG model is given by:

$$u_{\hat{d}} = -\hat{R}_s i_{\hat{d}} - L_{\hat{d}}\frac{di_{\hat{d}}}{dt} + L_{\hat{q}} i_{\hat{q}} \omega_e, \tag{7}$$

$$u_{\hat{q}} = -\hat{R}_s i_{\hat{q}} - L_{\hat{q}}\frac{di_{\hat{q}}}{dt} + (-L_{\hat{d}} i_{\hat{d}} + \Psi_{\hat{m}})\omega_e. \tag{8}$$

With the PMSG, $L_{\hat{d}} = L_{\hat{q}}$, which will refer to $\hat{L}$ for both quantities. Altered (7) and (8), it gives:

$$\frac{di_{\hat{d}}}{dt} = -\frac{\hat{R}_s}{\hat{L}} i_{\hat{d}} + \omega_e i_{\hat{q}} - \frac{1}{\hat{L}} u_{\hat{d}},$$

$$\frac{di_{\hat{q}}}{dt} = -\frac{\hat{R}_s}{\hat{L}} i_{\hat{q}} - \omega_e i_{\hat{d}} - \frac{1}{\hat{L}} u_{\hat{d}} + \frac{1}{\hat{L}} \Psi_{\hat{m}} \omega_e.$$

On the basis of the high-speed shaft rotational speed equation, the third state variable is defined as follows:

$$\frac{d\omega_r}{dt} = \frac{\tau_{\hat{m}}}{J} - \frac{\tau_e}{J} - \frac{\hat{B}\omega_r}{J}, \tag{9}$$

where, $\hat{B}\omega_r$ denotes the frictional damping torque. We can set $\hat{B} = 0$ if we disregard the damping friction torque.

The electrical rotational speed is $\omega_e = \frac{\hat{P}}{2}\omega_r$, where $\hat{P}$ denotes the stator pole count. To increase the electrical power extraction, a field-oriented control strategy is used, in which the electromechanical torque and rotor flux are independently controlled. The electric torque τ_e in (9) is defined as follows:

$$\tau_e = \frac{3}{2}\frac{\hat{P}}{2}\Psi_{\hat{m}} i_{\hat{q}} = \hat{k}_t i_{\hat{q}}, \tag{10}$$

where, $\hat{k}_t = \frac{3}{4}\hat{P}\Psi_{\hat{m}}$ is the torque coefficient. Therefore, the comprehensive PMSG-based WECS model is as described below: [32]:

$$\begin{bmatrix} \dot{i}_{\hat{d}}(t) \\ \dot{i}_{\hat{q}}(t) \\ \dot{\omega}_r(t) \end{bmatrix} = \begin{bmatrix} \frac{-\hat{R}_s}{\hat{L}} i_{\hat{d}} + \frac{\hat{P}}{2}\omega_r i_{\hat{q}} \\ \frac{-\hat{R}_s}{\hat{L}} - \frac{\hat{P}}{2}\omega_r i_{\hat{d}} + \frac{\Psi_{\hat{m}}\frac{\hat{P}}{2}\omega_r}{\hat{L}} \\ \frac{\tau_{\hat{m}}}{J} - \frac{3\hat{P}}{4J}\Psi_{\hat{m}} i_{\hat{q}} \end{bmatrix} + \begin{bmatrix} \frac{-1}{\hat{L}} & 0 \\ 0 & \frac{-1}{\hat{L}} \\ 0 & 0 \end{bmatrix} \begin{bmatrix} u_{\hat{d}} \\ u_{\hat{q}} \end{bmatrix}. \tag{11}$$

Linearized WECS Model. According to (4), the ideal mechanical speed of rotation is as follows:

$$\omega_r^* = \frac{\hat{\lambda}_o \hat{v}}{\hat{R}_t}. \tag{12}$$

Moreover, the optimal quadrature axis current $i_{\hat{q}}^*$ is defined as

$$i_{\hat{q}}^* = \frac{\hat{k}^*}{\hat{k}_t}(\omega_r^*)^2. \tag{13}$$

To maximize the produced electromechanical torque τ_e, it is preferred to align the stator current space vector with the quadrature axis (q-axis). This is because the q-axis is responsible for producing the torque that drives the rotation of the machine. This alignment can be achieved through the use of a field-oriented control strategy, where the current vector is divided into two components: one along the d-axis and one along the q-axis. In field-oriented control, the optimal direct axis current $i_{\hat{d}}^*$ is set to zero, which ensures that the stator current vector is aligned with the q-axis. This allows the maximum possible torque to be produced, resulting in improved performance of the machine. By using this strategy, the machine can operate more efficiently, with reduced losses and improved power output.

$$i_{\hat{d}}^* = 0. \tag{14}$$

To obtain a linearized model for the PMSG-based Wind Energy Conversion System (WECS), we begin by selecting a desired equilibrium point based on the optimal operating conditions, as specified in (12), (13), and (14). Then, we take the partial derivatives of the system dynamics (11) with respect to the state variables, evaluated at this equilibrium point. Using this approach, we can derive a linearized model for the system in the following form:

$$\begin{bmatrix} \dot{i}_{\hat{d}} \\ \dot{i}_{\hat{q}} \\ \dot{\omega}_r \end{bmatrix} = \begin{bmatrix} \frac{-\hat{R}_s}{\hat{L}} & \frac{\hat{P}\omega_r^*}{2} & \frac{\hat{P}i_{\hat{q}}^*}{2} \\ \frac{\hat{P}\omega_r^*}{2} & \frac{-\hat{R}_s}{\hat{L}} & \frac{4\hat{P}}{2\hat{L}} - \frac{\hat{P}i_{\hat{d}}^*}{2} \\ 0 & \frac{-\hat{P}\Psi_{\hat{m}}}{4J} & 0 \end{bmatrix} \begin{bmatrix} i_{\hat{d}} \\ i_{\hat{q}} \\ \omega_r \end{bmatrix} + \begin{bmatrix} \frac{-1}{\hat{L}} & 0 \\ 0 & \frac{-1}{\hat{L}} \\ 0 & 0 \end{bmatrix} \begin{bmatrix} u_{\hat{d}} \\ u_{\hat{q}} \end{bmatrix}. \tag{15}$$

A tachometer is a device used to measure the actual mechanical speed of rotation, denoted by ω_r, and provides this information in real-time to the control system. For a PMSG-based WECS, a linearized dynamical model can be constructed to capture the system dynamics, control, and external disturbances while accounting for feedback delay in ω_r and model uncertainty.

$$\begin{bmatrix} \dot{i}_{\hat{d}}(t) \\ \dot{i}_{\hat{q}}(t) \\ \dot{\omega}_r(t) \end{bmatrix} = \begin{bmatrix} g_1 & g_2 & 0 \\ -g_2 & g_1 & 0 \\ 0 & g_3 & 0 \end{bmatrix} \begin{bmatrix} i_{\hat{d}}(t) \\ i_{\hat{q}}(t) \\ \omega_r(t) \end{bmatrix} + \begin{bmatrix} 0 & 0 & \frac{\hat{P}i_{\hat{q}}^*}{2} \\ 0 & 0 & g_4 \\ 0 & 0 & 0 \end{bmatrix} \begin{bmatrix} i_{\hat{d}}(t-\tau(t)) \\ i_{\hat{q}}(t-\tau(t)) \\ \omega_r(t-\tau(t)) \end{bmatrix} + \begin{bmatrix} \frac{-1}{\hat{L}} & 0 \\ 0 & \frac{-1}{\hat{L}} \\ 0 & 0 \end{bmatrix} \begin{bmatrix} u_{\hat{d}} \\ u_{\hat{q}} \end{bmatrix} + \begin{bmatrix} 1 \\ 1 \\ 1 \end{bmatrix} w,$$

where,

$$g_1 = \frac{-\hat{R}_s + \Delta\hat{R}_s}{\hat{L} + \Delta\hat{L}},\ g_2 = \frac{\hat{P}\omega_r^*}{2},$$
$$g_3 = \frac{-3\hat{P}\Psi_{\hat{m}}}{4},\ g_4 = \frac{4\hat{P}}{2\hat{L} + \Delta\hat{L}} - \frac{\hat{P}i_{\hat{d}}^*}{2},$$

w denote the external disturbance term; $\Delta\hat{R}_s$ and $\Delta\hat{L}$ denote the resistance and inductance variations.

In this work, we look at a time-varying delay system that may be characterized by the differential equations below

$$\begin{aligned} \dot{\xi}(t) &= (A_0 + \Delta A_0)\xi(t) + (A_1 + \Delta A_1)\xi(t - d(t)) \\ &\quad + (B + \Delta B)u(t) + \bar{A}_2 w(t), \\ \xi(t) &= \hat{\phi}(t), \forall\, t \in [-d_2, -d_1] \end{aligned} \tag{16}$$

where $\xi(t) \in \mathbb{R}^n$, $u(t) \in \mathbb{R}^m$ states the state vector and the control input, respectively; $w(t) \in \mathbb{R}^q$ is the exogeneous disturbance $L_2 \in [0, \infty)$. A_0, A_1, B, and $\bar{A}_2$ are known constant matrices with approximate dimensions. $\hat{\phi}(t)$ indicates the initial condition in $[-d_2, 0]$. ΔA_0, ΔA_1, and ΔB are unknown matrices that are supposed to reflect the time-varying parameter uncertainty.

$$[\Delta A_0 \ \Delta A_1 \ \Delta B] = \mathcal{G}\mathcal{F}(t)[\mathcal{H}_1 \ \mathcal{H}_2 \ \mathcal{H}_3], \tag{17}$$

where the real constant matrices $\mathcal{G}, \mathcal{H}_1, \mathcal{H}_2, \mathcal{H}_3$ are known, and $\mathcal{F}(t)$ denotes an unknown time-varying matrix function.

$$\mathcal{F}^T(t)\mathcal{F}(t) \leq I. \tag{18}$$

During this whole work, we will look at the modeled system (16) stability issues in the presence of time-varying delays listed below. For all $t \geq 0$, the time-delay $d(t)$ is a differentiable function.

$$0 < d_1 \leq d(t) \leq d_2, \ \dot{d}(t) \leq h_d, \tag{19}$$

A. IMPACT OF TIME-DELAY ON STABILITY OF INVERTERS

The wide proliferation of power electronic systems with precise control systems requires implementation with microprocessor-based systems. The digital implementation of the pulse width modulation techniques requires a zero-order hold, which leads to a phase lag-induced time delay [33]. The one-step delay is utilized in digital control systems to sample the voltage or current signals precisely at the occurrence of a control interrupt. The impact of delay introduced by the digital controller has an impact on the system stability as well. The impact of control delay on the stability of the DC/AC inverter was systematically analyzed in [34]. With the inverter-side current taken as feedback, the change in time delay of one switching period T_s is sufficient to push the system out of stability. The impact of time delay on the closed-loop poles and zeros for a time delay variation of $0T_s$ to $3T_s$ is shown in Figure 3.

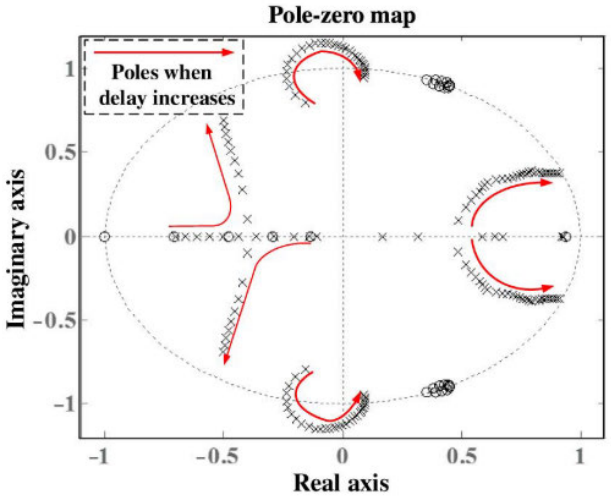

FIGURE 3. Impact of time delay on poles and zeros for an inverter [34].

The wind energy conversion systems utilize power electronic converters for AC/DC conversion and DC/AC conversion in a back-to-back type connection. These controlled converters deploy digital closed-loop control systems for output regulation and ripple reduction. The zero-order hold in the digital control systems is the primary source of phase lag-induced time delay. The grid-side inverter utilizes an LCL filter to reduce the harmonics in the current injected into the grid. The LCL filter has an inherent resonant issue that has to be actively damped. The performance of active damping systems is also severely impacted by the time delay [35]. The impact of time delay in the regulation of load frequency for three-area power systems is studied in [36], and a delay compensation mechanism is introduced to overcome the impact of time delay on the stability of load frequency control. Hence, there is a need to design digital control systems for power converters capable of providing delay-dependent stability [37].

With the increased penetration of renewable energy-based systems in the electric power grid, the requirement of power electronic systems for the conversion and control of electric power injection to the grid is also increasing. The increased utilization of power electronic converters Ingrid interfacing of renewable energy systems is slowly making the grid-forming converters. In this context, the stabilization of electronic converters exporting power to the grid in the time delay induced by digital control systems is of extreme importance.

B. DECENTRALIZED EVENT-TRIGGERED SCHEME

To reduce bandwidth consumption, a DETC is being used. The inputs d and measurement faults $\xi(t)$ are gathered into z nodes throughout this arrangement, furthermore, the signals associated with node $u \in \{1, 2, \ldots, z\}$ are indicated by $\xi_u(t)$ in $\mathbb{R}^n$ for $\sum_{u=1}^{z} d_u = d$. We signify u^{th} event generator discharge moments with $[t^u_{\bar{k}_u}\hat{h}]^{\infty}_{\bar{k}_u} = 0$ and verify every next release of event generator with $t^u_{\bar{k}_u+1}\hat{h}$ and u is calculated as follows:

$$\begin{aligned} t^u_{\bar{k}_u+1}\hat{h} = t^u_{\bar{k}_u}\hat{h} + \min\{p\hat{h} | Q_u^T(t^u_{\bar{k}_u}\hat{h} + p\hat{h})\phi_u Q_u(t^u_{\bar{k}_u}\hat{h} + p\hat{h}) \\ > \sigma_u \xi_u^T(t^u_{\bar{k}}\hat{h})\phi_u \xi_u(t^u_{\bar{k}}\hat{h}), \end{aligned} \tag{20}$$

where $\phi_u > 0, \sigma_u = 0$, and the difference between the latest sampling vector as well as the most recent transmission vector is defined as.

$$Q_u(t^u_{\bar{k}_u}\hat{h} + p\hat{h}) = \xi_u(t^u_{\bar{k}_u}\hat{h} + p\hat{h}) - \xi_u(t^u_{\bar{k}_u}\hat{h}).$$

We will look at a DETC, which is a crucial component for creating any control framework and reducing the network's communication cost. In general, from (20), the group of release instants $\{t^u_{\bar{k}u}\hat{h}\}$ is a subset of $\{0, \hat{h}, 2\hat{h}, \ldots\}$. The DETC approach is intended to be diminished certain unnecessary transmission of data. We are interested in constructing the controller below in this article.

$$u(t) = \tilde{K}[\xi_1^T(t^1_{\bar{k}_1}\hat{h}) \ \xi_2^T(t^2_{\bar{k}_2}\hat{h}) \ \ldots \ \xi_z^T(t^z_{\bar{k}_z}\hat{h})], t \in [t_{\bar{k}}\hat{h}, t_{\bar{k}+1}\hat{h}), \tag{21}$$

where the non-fragile controller gain is represented by ΔK and $\tilde{K} = K + \Delta K$. The following variations of the multiplicative non-fragile controller gains will be taken into consideration:

$$\Delta K = \mathcal{E}_0 F(t) \mathcal{E}_1 K, \tag{22}$$

the constant matrices $\mathcal{E}_0$ and $\mathcal{E}_1$ are of the required dimensions, and the unknown matrix function $F(t)$ has the condition

$$F^T(t)F(t) \leq I. \tag{23}$$

Moreover, construct $\eta_2(t) = t - t_{\bar{k}}\hat{h} - p\hat{h}$ for $t \in \rho_p$. It is easy to understand that $\eta_2(t)$ is a piecewise linear function satisfying

$$\begin{cases} 0 \leq \eta_2(t) \leq h_3, & t \in \rho_p, \\ \dot{\eta}_2(t) = 1, & t \neq t_{\bar{k}}\hat{h} + u\hat{h}. \end{cases}$$

Therefore, the threshold error $Q_u(t_{\bar{k}}\hat{h}+p\hat{h})$ can be rewritten as $Q_u(t-\eta_2(t)) = \xi_u(t-\eta_2(t)) - \xi_u(t^u_{\bar{k}_u}\hat{h}), \quad t \in \rho_p$.

Define the control input $u(t)$ as

$$u(t) = \tilde{K}(\xi(t-\eta_2(t)) - Q(t-\eta_2(t))), \quad t \in \rho_p. \tag{24}$$

Utilizing (24) in (16), we get

$$\begin{aligned} \dot{\xi}(t) = \bar{A}_0\xi(t) + \bar{A}_1\xi(t-d(t)) + \bar{A}_2 w(t) \\ + \bar{B}\tilde{K}(\xi(t-\eta_2(t)) - Q(t-\eta_2(t))), \end{aligned} \tag{25}$$

for $t \in \rho_p$. where, $\bar{A}_0 = A_0 + \Delta A_0$, $\bar{A}_1 = A_1 + \Delta A_1$, $\bar{B} = B + \Delta B$. From the DETC condition (20) that there exists for $t \in \rho_p$,

$$\begin{aligned} Q^T(t-\eta_2(t))\,\phi\, Q(t-\eta_2(t)) \leq \sigma\big[\xi(t-\eta_2(t)) \\ -Q(t-\eta_2(t))\big]^T \phi[\xi(t-\eta_2(t)) - Q(t-\eta_2(t))], \end{aligned}$$

with $\phi = \{\phi_1, \phi_2, \ldots, \phi_z\}$ and $\sigma = \{\sigma_1, \sigma_2, \ldots, \sigma_z\}$.

Remark 1: Note that the triggered setting off in (20) is decentralized. The sampling, triggering rules, and communication for any correspondence channel (e.g., u^{th} channel) just requires its own sampled details, and its event-triggered moments are unique in relation to different channels $(t^u_0\hat{h}, t^u_1\hat{h}, \ldots, t^u_{\bar{k}_u}\hat{h})$. Accordingly, contrasted with (20), this decentralized trigger makes additional degrees of freedom and is more productive.

Before we begin, we introduce essential definitions and lemmas to assist us in obtaining our important results.

Definition 2: [38] The system (25) stated that passive if there exists a scalar $\gamma > 0$ such that, $\forall t_p \geq 0$

$$2\left\{\int_0^{t_p} y^T(t)\phi_1(t)dt\right\} \geq -\gamma\left\{\int_0^{t_p} \phi_1^T(t)\phi_1(t)dt\right\},$$

under the zero initial condition satisifes, where $y^T(t) = \xi^T(t)$ and $\phi_1^T(t) = w^T(t)$.

Lemma 3: [39] The subsequent inequalities exist for any continuously differentiable functions $\xi : [a, b] \to \mathbb{R}$ for any positive-definite matrix $\mathbb{Z} > 0$ and scalars $a > 0$ such that $a < b$.

$$\int_a^b \int_\beta^b \dot{\xi}^T(s)\mathbb{Z}\dot{\xi}(s)dsd\beta \leq -2\Phi_1^T\mathbb{Z}\Phi_1 - 4\Phi_2^T\mathbb{Z}\Phi_2,$$
$$\int_a^b \int_a^\beta \dot{\xi}^T(s)\mathbb{Z}\dot{\xi}(s)dsd\beta \leq -2\Phi_3^T\mathbb{Z}\Phi_3 - 4\Phi_4^T\mathbb{Z}\Phi_4,$$

where

$$\begin{aligned} \Phi_1 &= \xi(b) - \frac{1}{b-a}\int_a^b \xi(s)ds, \ \Phi_2 = \xi(b) \\ &\quad + \frac{2}{b-a}\int_a^b \xi(s)ds \\ &\quad - \frac{6}{(b-a)^2}\int_a^b\int_\beta^b \xi(s)dsd\beta, \\ \Phi_3 &= \xi(a) - \frac{1}{b-a}\int_a^b \xi(s)ds, \\ \Phi_4 &= \xi(a) - \frac{4}{b-a}\int_a^b \xi(s)ds + \frac{6}{(b-a)^2}\int_a^b\int_\beta^b \xi(s)dsd\beta. \end{aligned}$$

Lemma 4: [40] For any semi-positive definite matrices

$$U = \begin{bmatrix} U_{11} & U_{12} & U_{13} \\ U_{12}^T & U_{22} & U_{23} \\ U_{13}^T & U_{23}^T & U_{33} \end{bmatrix}$$

≥ 0 the subsequent integral inequality satisfies:

$$\begin{aligned} -\int_{t-d(t)}^t \dot{\xi}^T(s)U_{33}\dot{\xi}(s)ds \leq \int_{t-d(t)}^t [\xi^T(t)\ \xi^T(t-d(t))\ \dot{\xi}^T s] \\ \begin{bmatrix} U_{11} & U_{12} & U_{13} \\ U_{12}^T & U_{22} & U_{23} \\ U_{13}^T & U_{23}^T & 0 \end{bmatrix} \begin{bmatrix} \xi(t) \\ \xi(t-d(t)) \\ \dot{\xi}(s) \end{bmatrix} ds. \end{aligned}$$

Lemma 5: [14] For block symmetric matrices $R = diag\{R_2, 3R_2, 5R_2\}$ with $T > 0$, any matrix S, the following inequality holds:

$$\begin{aligned} \psi(t) \leq -\frac{1}{h_3}\Upsilon^T(t)\begin{bmatrix} T_1 \\ T_2 \end{bmatrix}^T \left(\begin{bmatrix} R & S \\ * & R \end{bmatrix}\right. \\ \left. + \begin{bmatrix} \frac{h_3-\eta_2(t)}{h_3}U_1 & 0 \\ 0 & \frac{\eta_2(t)}{h_3}U_2 \end{bmatrix}\right) \begin{bmatrix} T_1 \\ T_2 \end{bmatrix} \Upsilon(t), \end{aligned}$$

where

$$\begin{aligned} \psi(t) &= -\int_{t-\eta_2(t)}^t \dot{\xi}^T(s)R_2\dot{\xi}(s)ds - \int_{t-h_3}^{t-\eta_2(t)} \dot{\xi}^T(s)R_2\dot{\xi}(s)ds \\ \Upsilon(t) &= [\xi^T(t)\ \xi^T(t-\eta_2(t))\ \xi^T(t-h_3)\ v_1^T(t)\ v_2^T(t)\ v_3^T(t)\ v_4^T(t)]^T, \\ b_j &= [0_{n\times(j-1)_n} \quad I \quad 0_{n\times(7-j)n}],\ j = 1, 2, \cdots, 7, \\ U_1 &= R - SR^{-1}S^T,\ U_2 = R - S^TR^{-1}S, \\ v_1(t) &= \frac{1}{\eta_2(t)}\int_{t-\eta_2(t)}^t \xi(s)ds, \end{aligned}$$

$$v_2(t) = \frac{1}{h_3 - \eta_2(t)} \int_{t-h_3}^{t-\eta_2(t)} \xi(s)ds,$$
$$v_3(t) = \frac{1}{\eta_2^2(t)} \int_{t-\eta_2(t)}^{t} \int_{s}^{t} \xi(\theta)d\theta ds,$$
$$v_4(t) = \frac{1}{(h_3 - \eta_2(t))^2} \int_{t-h_3}^{t-\eta_2(t)} \int_{s}^{t-\eta_2(t)} \xi(\theta)d\theta ds,$$
$$T_1 = \begin{bmatrix} b_1 - b_2 \\ b_1 + b_2 - 2b_4 \\ b_1 - b_2 + 6b_4 - 12b_6 \end{bmatrix}, \; T_2 = \begin{bmatrix} b_2 - b_3 \\ b_2 + b_3 - 2b_5 \\ b_2 - b_3 + 6b_5 - 12b_7 \end{bmatrix}.$$

Lemma 6: [24] Let $F(t)$ be a real matrix that satisfies $F^T(t)F(t) \leq I$. Additionally, let $\mathcal{E}_0$, $\mathcal{E}_1$, and $F(t)$ be real matrices with appropriate dimensions. Then, for any scalar $\epsilon > 0$, the subsequent inequality satisfies:

$$\mathcal{E}_0 F(t)\mathcal{E}_1 + \mathcal{E}_1^T F^T(t)\mathcal{E}_0^T \leq \epsilon^{-1}\mathcal{E}_0\mathcal{E}_0^T + \epsilon\mathcal{E}_1^T\mathcal{E}_1.$$

III. MAIN RESULTS

The key findings of this study reveal that our decentralized event-triggered approach ensures the overall system's stability. A new DDA for the system (25) is designed to achieve certain less conservative criteria. New stability standards for the interval time-varying delay system (25) are presented in the following theorem.

$$\eta^T(t) = \Big[\xi^T(t), \xi^T(t - d(t)), \xi^T(t - d_2), \xi^T(t - \alpha\delta), \xi^T(t - \eta_2(t)), \xi^T(t - h_3), \frac{1}{\eta_2(t)} \int_{t-\eta_2(t)}^{t} \xi^T(s)ds, \frac{1}{\eta_2^2(t)} \int_{t-\eta_2(t)}^{t} \int_{s}^{t} \xi^T(\theta)d\theta ds, \frac{1}{h_3 - \eta_2(t)} \int_{t-h_3}^{t-\eta_2(t)} \xi^T(s)ds, \frac{1}{(h_3 - \eta_2(t))^2} \int_{t-h_3}^{t-\eta_2(t)} \int_{s}^{t-\eta_2(t)} \xi^T(\theta)d\theta ds, \dot{\xi}^T(t), Q^T(t - \eta_2(t)), \frac{1}{\alpha\delta} \int_{t-\alpha\delta}^{t} \xi^T(s)ds, \frac{1}{(\alpha\delta)^2} \int_{-\alpha\delta}^{0} \int_{t+\theta}^{t} \xi^T(s)dsd\theta, \frac{1}{d_2 - \alpha\delta} \int_{t-d_2}^{t-\alpha\delta} \xi^T(s)ds, \frac{1}{(d_2 - \alpha\delta)^2} \int_{-d_2}^{-\alpha\delta} \int_{t+\theta}^{t} \xi^T(s)dsd\theta, w^T(t)\Big],$$
$$\Xi = \begin{bmatrix} \Xi_{11} & \Xi_{12} & \Xi_{13} \\ \Xi_{12}^T & \Xi_{22} & \Xi_{23} \\ \Xi_{13}^T & \Xi_{23}^T & \Xi_{33} \end{bmatrix} \geq 0, \; \Xi = U, \; V, \; W.$$

Theorem 7: According to Definition 2, the system (25) under the influence of (19) is regarded as passivity. In addition to the gain $\tilde{K}$, this is true for the following scalar parameters: $0 < d_1 \leq d(t) \leq d_2$, α $(0 < \alpha < 1)$, σ, γ, h_3, and $h_d > 0$. The positive-definite matrices P, Q_i, and $R_j(i = 1, 2, 3, 4, 5; j = 1, 2, 3, 4, 5, 6, 7)$, semi-positive definite matrices Ξ_{11}, Ξ_{12}, Ξ_{13}, Ξ_{22}, Ξ_{23}, Ξ_{33}, real matrix L, and matrix $\phi > 0$ with the proper dimensions satisfy the passivity conditions, subsequent LMIs satisfy with $\eta_2(t) \in [0, h_3]$:

$$\theta < 0 \tag{26}$$

and

$$\begin{aligned} Q_4 - U_{33} &\geq 0, \\ Q_5 - V_{33} &\geq 0, \\ Q_5 - W_{33} &\geq 0 \end{aligned} \tag{27}$$

where $\theta = [\theta_{ij}]_{17\times 17}$ (see Appendix)

Proof: Based on the DDA at the midpoint δ, we divide the delay interval over two equivalent sub-intervals (i.e., equivalent to $[d_1, \delta]$ and $[\delta, d_2]$). If we can show that Theorem 7 holds for two situations, $\alpha\delta \leq d(t) \leq d_2$ and $d_1 \leq d(t) \leq \alpha\delta$, where $\delta = (d_2 + d_1)/2$, then Theorem 7 is true.

Case 1: When $\alpha\delta \leq d(t) \leq d_2$, construct a Lyapunov-Krasovski functional (LKF) candidate as

$$V(\xi(t)) = \sum_{r=1}^{7} V_r(\xi(t)) \tag{28}$$

where

$$V_1(\xi_t) = \xi^T(t)P\xi(t),$$
$$V_2(\xi_t) = \int_{t-\alpha\delta}^{t} \xi^T Q_1\xi(s)ds + \int_{t-d_2}^{t} \xi^T(s)Q_2\xi(s)ds + \int_{t-d(t)}^{t} \xi^T(s)Q_3\xi(s)ds,$$
$$V_3(\xi_t) = \int_{-\alpha\delta}^{0} \int_{t+\theta}^{t} \dot{\xi}^T(s)Q_4\dot{\xi}(s)dsd\theta + \int_{-d_2}^{-\alpha\delta} \int_{t+\theta}^{t} \dot{\xi}^T(s)Q_5\dot{\xi}(s)dsd\theta,$$
$$V_4(\xi_t) = \int_{t-\eta_2(t)}^{t} \xi^T(s)R_1\xi(s)ds + h_3 \int_{-h_3}^{0} \int_{t+\theta}^{t} \dot{\xi}^T(s)R_2\dot{\xi}(s)dsd\theta,$$
$$V_5(\xi_t) = h_3^2 \int_{t-\eta_2(t)}^{t} \dot{\xi}^T(s)R_3\dot{\xi}(s)ds - \frac{\pi^2}{4} \int_{t-\eta_2(t)}^{t} [\xi^T(s) - \xi^T(t - \eta_2(t))]R_3 \times [\xi(s) - \xi(t - \eta_2(t))]ds,$$
$$V_6(\xi_t) = \int_{-\alpha\delta}^{0} \int_{-\alpha\delta}^{\theta} \int_{t+\beta}^{t} \dot{\xi}^T(s)R_4\dot{\xi}(s)dsd\beta d\theta + \int_{-\alpha\delta}^{0} \int_{\theta}^{0} \int_{t+\beta}^{t} \dot{\xi}^T(s)R_5\dot{\xi}(s)dsd\beta d\theta,$$
$$V_7(\xi_t) = \int_{-d_2}^{-\alpha\delta} \int_{-d_2}^{\theta} \int_{t+\beta}^{t} \dot{\xi}^T(s)R_6\dot{\xi}(s)dsd\beta d\theta$$

$$+\int_{-d_2}^{-\alpha\delta}\int_{\theta}^{-\alpha\delta}\int_{t+\beta}^{t}\dot{\xi}^T(s)R_7\dot{\xi}(s)ds d\beta d\theta.$$

The derivative of (28) with regard to $t > 0$ along the trajectories of (25) yields

$$\begin{aligned}
\dot{V}_1(\xi_t) &= 2\xi^T(t)P\dot{\xi}(t),\\
\dot{V}_2(\xi_t) &= \xi^T(Q_1+Q_2+Q_3)\xi(t) - \xi^T(t-\alpha\delta)Q_1\xi(t-\alpha\delta)\\
&\quad - \xi^T(t-d_2)Q_2\xi(t-d_2)\\
&\quad - \xi^T(t-d(t))(1-h_d)Q_3\xi(t-d(t)),\\
\dot{V}_3(\xi_t) &= \dot{\xi}^T(t)[Q_4(\alpha\delta)+Q_5(d_2-\alpha\delta)]\dot{\xi}(t)\\
&\quad - \int_{t-\alpha\delta}^{t}\dot{\xi}^T(s)Q_4\dot{\xi}(s)ds - \int_{t-d_2}^{t-\alpha\delta}\dot{\xi}^T(s)Q_5\dot{\xi}(s)ds,\\
\dot{V}_4(\xi_t) &= \xi^T(t)R_1\xi(t) + h_3^2\dot{\xi}^T(t)R_2\dot{\xi}(t)\\
&\quad - h_3\Big(\int_{t-\eta_2(t)}^{t}\dot{\xi}^T(s)R_2\dot{\xi}(s)ds\\
&\quad + \int_{t-h_3}^{t-\eta_2(t)}\dot{\xi}^T(s)R_2\dot{\xi}(s)ds\Big),\qquad (29)\\
\dot{V}_5(\xi_t) &= h_3^2[\dot{\xi}^T(t)R_3\dot{\xi}(t)]\\
&\quad - \frac{\pi^2}{4}\Big[\xi^T(t)R_3\xi(t) - \xi^T(t)R_3\xi(t-\eta_2(t))\\
&\quad - \xi^T(t-\eta_2(t))R_3\xi(t) + \xi^T(t-\eta_2(t))R_3\xi(t-\eta_2(t))\Big],\\
\dot{V}_6(\xi_t) &= \frac{(\alpha\delta)^2}{2}\dot{\xi}^T(t)(R_4\\
&\quad + R_5)\dot{\xi}(t) - \int_{-\alpha\delta}^{0}\int_{t-\alpha\delta}^{t+\theta}\dot{\xi}^T(s)R_4\dot{\xi}(s)ds d\theta\\
&\quad - \int_{-\alpha\delta}^{0}\int_{t+\theta}^{t}\dot{\xi}^T(s)R_5\dot{\xi}(s)ds d\theta,\\
\dot{V}_7(\xi_t) &= \frac{(d_2-\alpha\delta)^2}{2}\dot{\xi}^T(t)(R_6+R_7)\dot{\xi}(t)\\
&\quad - \int_{-d_2}^{-\alpha\delta}\int_{t-d_2}^{t+\theta}\dot{\xi}^T(s)R_6\dot{\xi}(s)ds d\theta\\
&\quad - \int_{d_2}^{-\alpha\delta}\int_{t+\theta}^{t-\alpha\delta}\dot{\xi}^T(s)R_7\dot{\xi}(s)ds d\theta.\qquad (30)
\end{aligned}$$

Utilizing Lemma 3, we computed as follows

$$\begin{aligned}
&-\int_{-\alpha\delta}^{0}\int_{t-\alpha\delta}^{t+\theta}\dot{\xi}^T(s)R_4\dot{\xi}(s)ds d\theta \le -\eta^T(t)E_1^T\hat{R}_4E_1\eta(t),\\
&-\int_{-\alpha\delta}^{0}\int_{t+\theta}^{t}\dot{\xi}^T(s)R_5\dot{\xi}(s)ds d\theta \le -\eta^T(t)E_2^T\tilde{R}_5E_2\eta(t),\\
&-\int_{-d_2}^{-\alpha\delta}\int_{t-d_2}^{t+\theta}\dot{\xi}^T(s)R_6\dot{\xi}(s)ds d\theta \le -\eta^T(t)E_3^T\tilde{R}_6E_3\eta(t),\\
&-\int_{d_2}^{-\alpha\delta}\int_{t+\theta}^{t-\alpha\delta}\dot{\xi}^T(s)R_7\dot{\xi}(s)ds d\theta \le -\eta^T(t)E_4^T\tilde{R}_7E_4\eta(t),
\end{aligned}$$

where

$$\tilde{R}_i = diag\{2R_i\ \ 4R_i\},\ i=4,5,6,7,$$

$$E_1 = \begin{bmatrix} a_4 - a_{13} \\ a_4 - 4a_{13} + 6a_{14} \end{bmatrix},\ E_2 = \begin{bmatrix} a_1 - a_{13} \\ a_1 + 2a_{13} - 6a_{14} \end{bmatrix},$$

$$E_3 = \begin{bmatrix} a_3 - a_{15} \\ a_3 - 4a_{15} + 6a_{16} \end{bmatrix},\ E_4 = \begin{bmatrix} a_4 - a_{15} \\ a_4 + 2a_{15} - 6a_{16} \end{bmatrix}.$$

Alternatively, the following inequalities are true

$$\begin{aligned}
&-\int_{t-\alpha\delta}^{t}\dot{\xi}^T(s)Q_4\dot{\xi}(s)ds - \int_{t-d_2}^{t-\alpha\delta}\dot{\xi}^T(s)Q_5\dot{\xi}(s)ds\\
&= -\int_{t-\alpha\delta}^{t}\dot{\xi}^T(s)Q_4\dot{\xi}(s)ds - \int_{t-d(t)}^{t-\alpha\delta}\dot{\xi}^T(s)Q_5\dot{\xi}(s)ds\\
&\quad - \int_{t-d_2}^{t-d(t)}\dot{\xi}^T(s)Q_5\dot{\xi}(s)ds,\\
&= -\int_{t-\alpha\delta}^{t}\dot{\xi}^T(s)U_{33}\dot{\xi}(s)ds - \int_{t-d(t)}^{t-\alpha\delta}\dot{\xi}^T(s)V_{33}\dot{\xi}(s)ds\\
&\quad - \int_{t-d_2}^{t-d(t)}\dot{\xi}^T(s)W_{33}\dot{\xi}(s)ds - \int_{t-\alpha\delta}^{t}\dot{\xi}^T(s)(Q_4-U_{33})\dot{\xi}(s)ds\\
&\quad - \int_{t-d(t)}^{t-\alpha\delta}\dot{\xi}^T(s)(Q_5-V_{33})\dot{\xi}(s)ds\\
&\quad - \int_{t-d_2}^{t-d(t)}\dot{\xi}^T(s)(Q_5-W_{33})\dot{\xi}(s)ds,\qquad (31)
\end{aligned}$$

Using Lemma 4 and the Leibniz-Newton formula, we get

$$\begin{aligned}
&-\int_{t-\alpha\delta}^{t}\dot{\xi}^T(s)U_{33}\dot{\xi}(s)ds = \xi^T[U_{11}(\alpha\delta)+U_{13}^T+U_{13}]\xi(t)\\
&\quad + \xi^T(t-\alpha\delta)[U_{12}^T(\alpha\delta)-U_{13}^T+U_{23}]\xi(t)\\
&\quad + \xi^T(t)[U_{12}(\alpha\delta)+U_{23}^T-U_{13}]\xi(t-\alpha\delta)\\
&\quad + \xi^T(t-\alpha\delta)[U_{22}(\alpha\delta)-U_{23}^T-U_{23}]\xi(t-\alpha\delta).\qquad (32)
\end{aligned}$$

Similarly

$$\begin{aligned}
&-\int_{t-d(t)}^{t-\alpha\delta}\dot{\xi}^T(s)V_{33}\dot{\xi}(s)ds = \xi^T(t-\alpha\delta)[V_{11}(d_2-\alpha\delta)\\
&\quad + V_{13}+V_{13}^T]\xi(t-\alpha\delta) + \xi^T(t-d(t))[V_{12}^T(d_2-\alpha\delta)\\
&\quad - V_{13}^T+V_{23}]\xi(t-\alpha\delta) + \xi^T(t-\alpha\delta)[V_{12}(d_2-\alpha\delta)\\
&\quad + V_{23}^T-V_{13}]\xi(t-d(t))\\
&\quad + \xi^T(t-d(t))[V_{22}(d_2-\alpha\delta)-V_{23}^T-V_{23}]\xi(t-d(t)),\qquad (33)
\end{aligned}$$

and

$$\begin{aligned}
&-\int_{t-d_2}^{t-d(t)}\dot{\xi}^T(s)W_{33}\dot{\xi}(s)ds\\
&= \xi^T(t-d(t))[W_{11}(d_2-\alpha\delta)+W_{13}^T+W_{13}]\xi(t-d(t))\\
&\quad + \xi^T(t-d_2)[W_{12}^T(d_2-\alpha\delta)-W_{13}^T+W_{23}]\xi(t-d(t))\\
&\quad + \xi^T(t-d(t))[W_{12}(d_2-\alpha\delta)+W_{23}^T-W_{13}]\xi(t-d_2)\\
&\quad + \xi^T(t-d_2)[W_{22}(d_2-\alpha\delta)-W_{23}^T-W_{23}]\xi(t-d_2).\qquad (34)
\end{aligned}$$

By applying Lemma 5, we proceed to compute the two single integral terms present in $\dot{V}_4(\xi_t)$ and the integral terms are effectively evaluated, allowing us to express $\dot{V}_4(\xi_t)$ in a

more analytically in the subsequent form

$$\psi(t) \le -\Upsilon^T(t)\begin{bmatrix} T_1 \\ T_2 \end{bmatrix}^T \left(\begin{bmatrix} R & S \\ * & R \end{bmatrix} + \begin{bmatrix} \frac{h_3-\eta_2(t)}{h_3}U_1 & 0 \\ 0 & \frac{\eta_2(t)}{h_3}U_2 \end{bmatrix} \right) \begin{bmatrix} T_1 \\ T_2 \end{bmatrix} \Upsilon(t) \quad (35)$$

where $\Upsilon(t)$, T_1, T_2, U_1, and U_2 are defined in Lemma 5.

Furthermore, the subsequent condition is met for each matrix $L = P$ with suitable dimensions:

$$2[\xi^T(t)L + \dot{\xi}^T(t)L][\bar{A}_0\xi(t) + \bar{A}_1\xi(t-d(t)) + \bar{A}_2 w(t) + \bar{B}\tilde{K}(\xi(t-\eta_2(t)) - Q(t-\eta_2(t))) - \dot{\xi}(t)] = 0. \quad (36)$$

where $\bar{A}_0, \bar{A}_1, \bar{B}$ is defined in (25). Using the last target to demonstrate the nonattendance of passive property, the following inequality is given:

$$\mathcal{J}(t_p) = 2\left\{ \int_0^{t_p} y^T(t)\phi_1(t)dt \right\} \ge -\gamma \left\{ \int_0^{t_p} \phi_1^T(t)\phi(t)dt \right\}$$
$$\Rightarrow -2\left\{ \int_0^{t_p} y^T(t)\phi_1(t)dt \right\} - \gamma \left\{ \int_0^{t_p} \phi_1^T(t)\phi_1(t)dt \right\} \le 0$$
$$\mathcal{J}(t_p) = \left\{ \int_0^{t_p} -2y^T(t)\phi_1(t) - \gamma\phi_1^T(t)\phi_1(t) \right\}. \quad (37)$$

By combining (29)-(37) it can be got that

$$\left\{ V(\xi_t) - 2y^T(t)\phi_1(t) - \gamma\phi_1^T(t)\phi_1(t) \right\} \le \{\eta^T(t)\theta\eta(t)\} < 0, \quad (38)$$

where, θ is defined in (26). Integrating both sides of (38) w.r.t $'t'$ over the period 0 to t_p

$$2\left\{ \int_0^{t_p} y^T(t)\phi_1(t)dt \right\} \ge \left\{ \int_0^{t_p} (V(\xi_t) - \gamma\phi_1^T(t)\phi_1(t))dt \right\},$$
$$\ge -\gamma \left\{ \int_0^{t_p} \phi_1^T(t)\phi_1(t))dt \right\}.$$

Since $Q_4 - U_{33} \ge 0$, $Q_5 - V_{33} \ge 0$ and $Q_5 - W_{33} \ge 0$ then the last three terms in (31) is less then or equal to 0. As a result, the system (25), which includes an interval time-varying delay, meets the requirements for passivity in accordance with Definition 2.

Case 2. When $d_1 \le d(t) \le \alpha\delta$, the LKF is chosen as follows:

$$V(\xi_t) = \xi^T(t)P\xi(t) + \int_{t-\alpha\delta}^{t} \xi^T(s)Q_1\xi(s)ds + \int_{t-d_1}^{t} \xi^T(s)Q_2\xi(s)ds + \int_{t-d(t)}^{t} \xi^t\xi^T(s)Q_3\xi(s)ds + \int_{-\alpha\delta}^{0}\int_{t+\theta}^{t} \dot{\xi}^T(s)Q_4\dot{\xi}(s)dsd\theta + \int_{-\alpha\delta}^{-d_1}\int_{t+\theta}^{t} \dot{\xi}^T(s)Q_5\dot{\xi}(s)dsd\theta + \int_{t-\eta_2(t)}^{t} \xi^T(s)R_1\xi(s)ds + h_3\int_{-h_3}^{0}\int_{t+\theta}^{t} \dot{\xi}^T(s)R_2\dot{\xi}(s)dsd\theta + h_3^2\int_{t-\eta_2(t)}^{t} \dot{\xi}^T(s)R_3\dot{\xi}(s)ds, - \frac{\pi^2}{4}\int_{t-\eta_2(t)}^{t} [\xi^T(s) - \xi^T(t-\eta_2(t))]R_3[\xi(s) - \xi(t-\eta_2(t))]ds + \int_{-\alpha\delta}^{0}\int_{-\alpha\delta}^{\theta}\int_{t+\beta}^{t} \dot{\xi}^T(s)R_4\dot{\xi}(s)dsd\beta d\theta + \int_{-\alpha\delta}^{0}\int_{\theta}^{0}\int_{t+\beta}^{t} \dot{\xi}^T(s)R_5\dot{\xi}(s)dsd\beta d\theta + \int_{-\alpha\delta}^{-d_1}\int_{-\alpha\delta}^{\theta}\int_{t+\beta}^{t} \dot{\xi}^T(s)R_6\dot{\xi}(s)dsd\beta d\theta + \int_{-\alpha\delta}^{-d_1}\int_{\theta}^{-d_1}\int_{t+\beta}^{t} \dot{\xi}^T(s)R_7\dot{\xi}(s)dsd\beta d\theta. \quad (39)$$

where $P > 0$, $Q_i > 0$, $R_j > 0$ $(i = 1, 2, 3, 4, 5;$ $j = 1, 2, 3, 4, 5, 6, 7)$. Choosing

$$\eta^T(t) = \Big[\xi^T(t), \xi^T(t-d(t)), \xi^T(t-\alpha\delta), \xi^T(t-d_1), \xi^T(t-\eta_2(t)), \xi^T(t-h_3), (\frac{1}{\eta_2(t)}\int_{t-\eta_2(t)}^{t} \xi(s)ds)^T, (\frac{1}{\eta_2^2(t)}\int_{t-\eta_2(t)}^{t}\int_{s}^{t} \xi(\theta)d\theta ds)^T, (\frac{1}{h_3-\eta_2(t)}\int_{t-h_3}^{t-\eta_2(t)} \xi(s)ds)^T, (\frac{1}{(h_3-\eta_2(t))^2}\int_{t-h_3}^{t-\eta_2(t)}\int_{s}^{t-\eta_2(t)} \xi(\theta)d\theta ds)^T, \dot{\xi}^T(t), Q^T(t-\eta_2(t)), (\frac{1}{\alpha\delta}\int_{t-\alpha\delta}^{t} \xi(s)ds)^T, (\frac{1}{(\alpha\delta)^2}\int_{-\alpha\delta}^{0}\int_{t+\theta}^{t} \xi(s)dsd\theta)^T, (\frac{1}{\alpha\delta-d_1}\int_{t-\alpha\delta}^{t-d_1} \xi(s)ds)^T, (\frac{1}{(\alpha\delta-d_1)^2}\int_{-\alpha\delta}^{-d_1}\int_{t+\theta}^{t} \xi(s)dsd\theta)^T, w^T(t)\Big].$$

and (26) − (27) as that for case 1.

Remark 8: Before stating the following theorem, it is pointed out that the non-fragile controller with uncertain parameters ΔB rarely happened simultaneously, despite the fact that it is a very practical problem [41], [42], [43]. Therefore, studying the non-fragility of the controller can be better applied and practiced.

Theorem 9: System (25) subject to (19) is passivity in the sense of Definition 2 and for given scalars $0 < d_1 \le d(t) \le d_2$, α $(0 < \alpha < 1)$, σ, γ, h_3, and $h_d > 0$, control gain K, if there exist positive-definite matrices P,

Q_i, R_j ($i = 1, 2, 3, 4, 5; j = 1, 2, 3, 4, 5, 6, 7$), semi-positive definite matrices Ξ_{11}, Ξ_{12}, Ξ_{13}, Ξ_{22}, Ξ_{23}, Ξ_{33}, real matrix L, if there exist scalars $\epsilon_1 > 0$, $\epsilon_2 > 0$, and matrix $\phi > 0$ with appropriate dimensions, such that the subsequent LMIs are satisfy with $\eta_2(t) \in [0, h_3]$:

$$\theta_1 < 0, \tag{40}$$

where

$$\theta_1 = \begin{bmatrix} \bar{\theta}_V & \Gamma_3 & \Gamma_4^T \\ * & -\epsilon_2 I & 0 \\ * & * & -\epsilon_2^{-1} I \end{bmatrix}, \ \bar{\theta}_V = \begin{bmatrix} \hat{\Pi} & \Gamma_1 & \Gamma_2^T \\ * & -\epsilon_1 I & 0 \\ * & * & -\epsilon_1^{-1} I \end{bmatrix},$$

and

$$\begin{aligned} Q_4 - U_{33} &\geq 0, \\ Q_5 - V_{33} &\geq 0, \\ Q_5 - W_{33} &\geq 0 \end{aligned} \tag{41}$$

where $\hat{\Pi} = [\hat{\theta}]_{17\times 17}$ (see Appendix)

Proof: From Theorem 7, it can be obtained easily that $\theta = \tilde{\theta} + \Delta\tilde{\theta}$. Then by Lemma 6, there exists $\epsilon_1 > 0$, such that

$$\Delta\tilde{\theta} = \Gamma_1 \mathcal{F}(t) \Gamma_2 + (\Gamma_1 \mathcal{F}(t) \Gamma_2)^T \leq \epsilon_1^{-1} \Gamma_1 \Gamma_1^T + \epsilon_1 \Gamma_2^T \Gamma_2$$

Utilizing the Schur complement, we have

$$\hat{\theta}_V = \begin{bmatrix} \tilde{\theta} & \Gamma_1 & \Gamma_2^T \\ * & -\epsilon_1 I & 0 \\ * & * & -\epsilon_1^{-1} I \end{bmatrix} < 0$$

where $\tilde{\theta} = [\tilde{\tilde{\theta}}_{ij}]_{17\times 17}$, and

$$\tilde{\tilde{\theta}}_{1,5} = 3R_2 + \frac{h_3 - \eta_2(t)}{h_3} 3R_2 + R_3 \frac{\pi^2}{4} + LB\tilde{K},$$
$$\tilde{\tilde{\theta}}_{1,12} = -LB\tilde{K}, \ \tilde{\tilde{\theta}}_{5,11} = (LB\tilde{K})^T, \ \tilde{\tilde{\theta}}_{11,12} = -LB\tilde{K}.$$

The other elements of $[\tilde{\tilde{\theta}}_{ij}]_{17\times 17}$ are same as in $[\theta]_{17\times 17}$. Moreover,

$$\Gamma_1 = [\mathcal{G}^T L^T \ \underbrace{0, \cdots, 0}_{9 \text{ times}} \ \mathcal{G}^T L^T \ \underbrace{0, \cdots, 0}_{6 \text{ times}}]^T,$$
$$\Gamma_2 = [\mathcal{H}_1 \ \mathcal{H}_2 \ 0 \ 0 \ \mathcal{H}_3 K \ \underbrace{0, \cdots, 0}_{6 \text{ times}} - \mathcal{H}_3 K \ \underbrace{0, \cdots, 0}_{5 \text{ times}}].$$

From non-fragile controller (21), we can see that

$$\hat{\theta}_V = \bar{\theta}_V + \Delta\bar{\theta}_V,$$

where $\bar{\theta}_V$ is the matrix, and switch the $\tilde{K}$ in $\hat{\theta}_V$ to K, considering (22) and Lemma 6, there exists scalars $\epsilon_2 > 0$, such that

$$\bar{\theta}_V + \Delta\bar{\theta}_V = \bar{\theta}_V + \Gamma_3 F(t) \Gamma_4 + (\Gamma_3 F(t) \Gamma_4)^T,$$
$$\leq \bar{\theta}_V + \epsilon_2 \Gamma_4^T \Gamma_4 + \epsilon_2^{-1} \Gamma_3 \Gamma_3^T. \tag{42}$$

Utilizing Schur complement, (42) is identical to (40), and the statement of the theorem is valid using the same argument as Theorem 7. This completed the proof. □

Depending on Theorem 9, we may build the controller (21) for the system (25), and K is the controller gain that must be computed.

IV. CONTROLLER DERIVATIONS

This section covers determining appropriate control gains to stabilize the performance of the investigated closed-loop system (25).

Theorem 10: System (25) subject to (19) is passivity in a manner of Definition 2 and for given scalars $0 < d_1 \leq d(t) \leq d_2$, α ($0 < \alpha < 1$), σ, h_3, γ, and $h_d > 0$, the matrices are exist with $\mathcal{X} > 0$, $\hat{Q}_i > 0$, $\hat{R}_j > 0$ ($i = 1, 2, 3, 4, 5; j = 1, 2, 3, 4, 5, 6, 7$), semi-positive definite matrices $\hat{\Xi}_{11}$, $\hat{\Xi}_{12}$, $\hat{\Xi}_{13}$, $\hat{\Xi}_{22}$, $\hat{\Xi}_{23}$, $\hat{\Xi}_{33}$ all are exists, matrix Y with appropriate dimensions, if there exist scalars $\epsilon_1 > 0, \epsilon_2 > 0$, and matrix $\phi > 0$ with appropriate dimensions, the subsequent conditions hold with $\eta_2(t) \in [0, h_3]$:

$$\hat{\Psi} < 0, \tag{43}$$
$$\begin{aligned} \hat{Q}_4 - \hat{U}_{33} &\geq 0, \\ \hat{Q}_5 - \hat{V}_{33} &\geq 0, \\ \hat{Q}_5 - \hat{W}_{33} &\geq 0 \end{aligned} \tag{44}$$

where $\hat{\Psi} = (\hat{\Psi}_{ij})_{21\times 21}$ (see Appendix)

Furthermore, the controller gain may be built as $K = Y\mathcal{X}^{-1}$.

Proof: Define $\mathcal{X} = P^{-1}$, $\hat{Q}_i = \mathcal{X} Q_i \mathcal{X}$, $\hat{R}_j = \mathcal{X} R_j \mathcal{X} (i = 1, 2, 3, 4, 5; j = 1, 2, 3)$, $\hat{U}_{lm} = \mathcal{X} U_{lm} \mathcal{X}$, $\hat{V}_{lm} = \mathcal{X} V_{lm} \mathcal{X}$, $\hat{W}_{lm} = \mathcal{X} W_{lm} \mathcal{X} (l = 1, 2; m = 1, 2, 3)$. Pre- and post-multiplying (40) with $diag\{\underbrace{\mathcal{X}, \ \mathcal{X}, \ \mathcal{X}}_{16 \text{ times}}, I, I, I, I, I\}$, and (27) with $\mathcal{X}$, we can obtain LMIs (43) and (44).

Remark 11: This paper introduces a novel relaxed integral inequality for estimating a single integral term while performing passivity analysis on the PMSG model with a time-varying delay. The relaxed integral inequality in Lemma 5 is advantageous because it makes it easier to figure out $\psi(t)$ without requiring any additional decision variables. As a result, when the two steps are considered together, the estimation has less conservatism than when the two steps are considered separately.

Remark 12: Compared to traditional centralized event-triggered control (CETC) schemes, the proposed DETC offers several key advantages in the context of PMSG-based WECS. In CETC frameworks, the triggering condition is evaluated using global system information, requiring all subsystem states to be continuously communicated to a central controller. This centralized structure incurs high communication overhead and is vulnerable to single-point failures and network-induced delays. In contrast, DETC allows each subsystem (node) $u \in \{1, 2, \ldots, z\}$ to independently monitor

its local measurement $\xi_u(t)$ and execute a local triggering condition of the form:

$$Q_u^T(t)\,\phi_u\,Q_u(t) > \sigma_u\,\xi_u^T(t_{\bar{k}_u}^u\hat{h})\,\phi_u\,\xi_u(t_{\bar{k}_u}^u\hat{h}), \tag{45}$$

where $\phi_u > 0$ and $\sigma_u \in [0,1)$ are tuning parameters that allow node-specific communication thresholds. This decentralized formulation reduces the frequency of unnecessary data transmissions and relaxes the reliance on synchronous communication. Furthermore, by accommodating asynchronous and delayed data updates, DETC improves robustness in real-time embedded WECS environments, where communication bandwidth is limited, and subsystems operate with partial observability and localized intelligence. Consequently, the DETC framework ensures scalability, fault tolerance, and efficient resource utilization, outperforming CETC under practical deployment conditions.

Remark 13: The proposed DETC scheme offers significant advancements over existing passivity-based control methods for wind turbine systems, particularly those focused on PMSG-based architectures. While prior works [31], [44] and [45] extensively explore passivity-based control for optimal power extraction and improved system robustness, they primarily operate under assumptions of continuous communication control structures. Similarly, [46] also presented a passivity-based control for a DFIG wind turbine, likely without detailed consideration of communication efficiency in a decentralized setting. Our approach distinguishes itself by integrating a novel DETC framework, which directly addresses the critical issue of network bandwidth consumption with passivity performance. Unlike the aforementioned passivity-based methods that typically rely on periodic sampling or continuous data exchange, our DETC mechanism intelligently selects data transmission instants.

In contrast, our work proposes a DETC scheme, where the triggering instants for each node are determined locally by checking the condition $Q_u^T(t_{\bar{k}_u}^u\hat{h} + p\hat{h})\phi_u Q_u(t_{\bar{k}_u}^u\hat{h} + p\hat{h}) > \sigma_u\xi_u^T(t_{\bar{k}}^u\hat{h})\phi_u\xi_u(t_{\bar{k}}^u\hat{h})$, where $\phi_u > 0$ and $\sigma_u = 0$ are design parameters. This decentralized triggering rule substantially reduces unnecessary data transmissions by transmitting sensor information only when the error exceeds a threshold relative to the measured state $\xi_u(t)$. Moreover, our proposed LKF explicitly incorporates both the upper and lower bounds of the time-varying delay $\tau(t)$, utilizing relaxed integral inequalities to enhance the accuracy and reduce conservatism of the passivity conditions. The resulting controller gain $\tilde{K} = K + \Delta K = \mathcal{E}_0F(t)\mathcal{E}_1K$ accounts for multiplicative non-fragile uncertainties, providing robustness against implementation errors and parameter variations. This integrated framework yields less conservative, delay-dependent LMI conditions for passivity, verified numerically, while achieving improved communication efficiency compared to the aforementioned studies.

Remark 14: The proposed DETC method presents several significant benefits: (i) It establishes specific triggering conditions for each event generator, enabling independent monitoring of local signals and decision-making regarding the transmission of updated measurements to the controller; and (ii) when the predefined threshold has been exceeded at event generator u, the relevant sensor data is sent to the controller asynchronously, ensuring that updates occur as necessary rather than in a synchronized fashion across all sensors.

V. NUMERICAL EVALUATIONS

Using the MATLAB programming environment and the parameters listed in the Table 4, numerical calculations are carried out to evaluate the efficacy of the DETC scheme in order to verify the generated PMSG.

The PMSG-based WECS is defined as follows:

$$\begin{aligned}\dot{\xi}(t) &= (A_0 + \Delta A_0)\xi(t) + (A_1 + \Delta A_1)\xi(t - d(t)) \\ &\quad + (B + \Delta B)u(t) + \bar{A}_2 w(t),\end{aligned} \tag{46}$$

where

$$A_0 = \begin{bmatrix} g_1 & g_2 & 0 \\ -g_2 & g_1 & 0 \\ 0 & g_3 & 0 \end{bmatrix},\ A_1 = \begin{bmatrix} 0 & 0 & \frac{Pi_q^*}{2} \\ 0 & 0 & g_4 \\ 0 & 0 & 0 \end{bmatrix},$$

$$B = \begin{bmatrix} \frac{-1}{L} & 0 \\ 0 & \frac{-1}{L} \\ 0 & 0 \end{bmatrix},\ \bar{A}_2 = \begin{bmatrix} 1 \\ 1 \\ 1 \end{bmatrix},$$

$$\mathcal{G} = 0.1,\ \mathcal{H}_1 = \mathcal{H}_2 = \mathcal{H}_3 = 0.1, \mathcal{E}_0,\ \mathcal{E}_1 = 0.2,$$

$$w(t) = 0.25\,e^{0.1\,sin(0.2t)}$$

The system parameters are taken as $h_d = 0.1$, $d_1 = 0.1$, $d_2 = 0.2$, $h_3 = 0.01$, and $\gamma = 0.1$. The MATLAB LMI toolbox can effectively handle the sufficient conditions listed in Theorem 10. The gain matrix and the triggered parameter are calculated as follows:

$$K = \begin{bmatrix} 3.02341 & 1.2341 & -0.4574 \\ -2.2412 & -2.0144 & 0.0074 \end{bmatrix},$$

$$\phi = \begin{bmatrix} 1.4720 & -0.1265 & -0.0147 \\ -0.1265 & 1.4712 & -0.0019 \\ -0.0147 & -0.0019 & 1.4675 \end{bmatrix}.$$

The controller design algorithm.

Input: Fix the parameters of the system (46).

Output: Gain matrices of the controller.

(1) Configure the proposed system parameters $\bar{A}_0$, $\bar{A}_1$, $\bar{A}_2$ and $\bar{B}$. Assume the event-triggered sample time is $h_3 = 0.05$ and the known scalars.

(2) With the appropriate equations (46). Utilizing the LMI toolbox in MATLAB and establishing the LMIs (43) and (44).

(3) Configure the bound values d_1 and d_2, as well as the constrained condition $d(t)$ and h_d.

(4) Modify the values of d_1 and d_2 to determine whether the LMI solution exists.

TABLE 3. Largest sampling interval h_3 when $d_2 = 0.2$.

Results	h_3	Gain matrices	Triggered parameters
Theorem 4.1	0.01	$K = \begin{bmatrix} 3.02341 & 1.2341 & -0.4574 \\ -2.2412 & -2.0144 & 0.0074 \end{bmatrix}$	$\phi = \begin{bmatrix} 1.4720 & -0.1265 & -0.0147 \\ -0.1265 & 1.4712 & -0.0019 \\ -0.0147 & -0.0019 & 1.4675 \end{bmatrix}$
Theorem 4.1	0.014	$K = \begin{bmatrix} 4.2514 & 2.1541 & -1.1245 \\ -2.7145 & -2.1241 & 0.0145 \end{bmatrix}$	$\phi = \begin{bmatrix} 1.4500 & 0.2414 & 0.0124 \\ 0.2414 & 1.4510 & -2.2301 \\ 0.0124 & -2.2301 & 1.4464 \end{bmatrix}$
Theorem 4.1	0.019	$K = \begin{bmatrix} 5.2415 & 2.2014 & -2.2847 \\ -3.2154 & -4.1052 & 0.2014 \end{bmatrix}$	$\phi = \begin{bmatrix} 8.7773 & -0.0030 & 0.0415 \\ -0.0030 & 8.8192 & 0.0102 \\ 0.0415 & 0.0102 & 8.7701 \end{bmatrix}$

TABLE 4. Parameters utilization for numerical computations.

$\hat{R}_s$	3.3 ω
$L_{\hat{d}} = L_{\hat{q}}$	41.56×10^{-3} H
$\hat{P}$	6
Ψ	0.4832 Wb
$\hat{\rho}$	1.25 kg/m^3
$\hat{R}_t$	2.5 m
$\hat{\lambda}_0$	7.2
$C_{\hat{p}}$	0.47
J	100 kg/m^2
$\hat{v}$	12 m/s
τ	0.01 s

(5) If there is a feasible solution, end the computation and receive the maximal number of d_2, the gains matrix K, and the triggering parameter ϕ; otherwise, return to step 4 and raise the values of d_2 and d_1.

(6) Stop.

Based on the above control gains and triggered parameters, the following simulations are discussed. Letting the randomized initial conditions, the simulation results on the state trajectories of the PMSG model without and with DETC are depicted, respectively, in Figures 4 and 5. From Figure 4, one can observe that system (46) without DETC may be inherently unstable. Moreover, Figure 5 confirms that when utilizing the DETC in (46), The PMSG model is effectively controlled and achieves robust passivity, even in the presence of uncertain parameters.

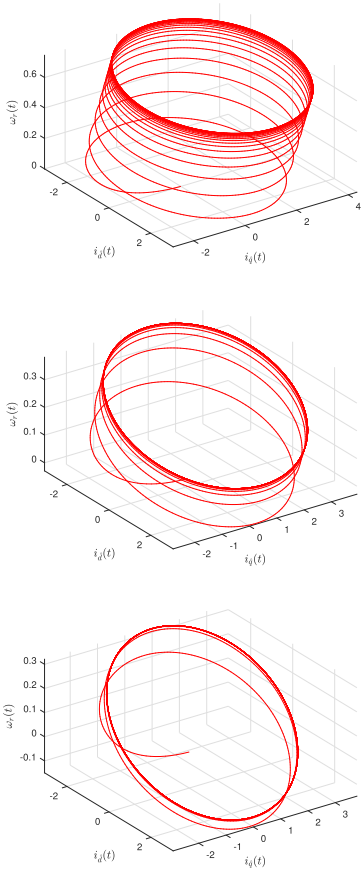

FIGURE 4. Behavior of the PMSG model (46) without control input for different kinds of value P (a) P = 2 (b) P = 3.3 (c) P = 4.5.

Figure 5 shows that when the system parameters fluctuate randomly within a particular range and the bound value is different, the control system can be promptly stabilized, and control performance and robustness are increased. Figure 4

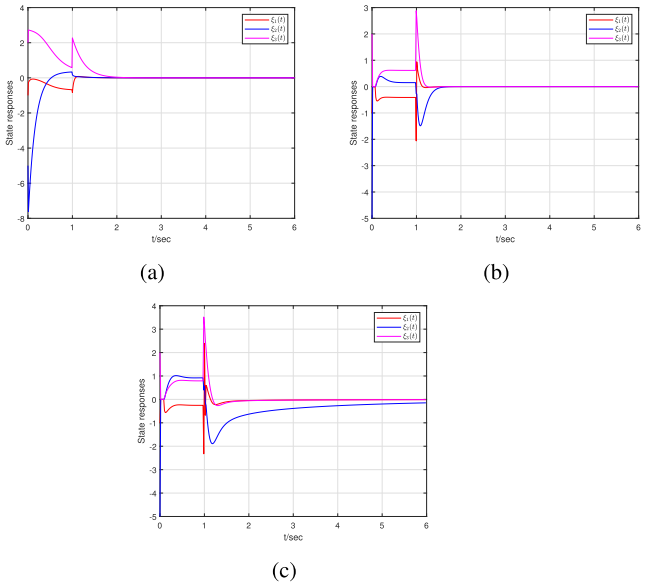

FIGURE 5. The given panels (a)-(c) depict the evolution of state response curves according to Table 3.

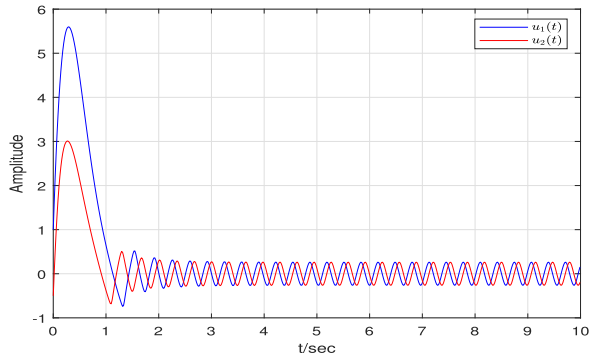

FIGURE 6. Control responses of the system (46).

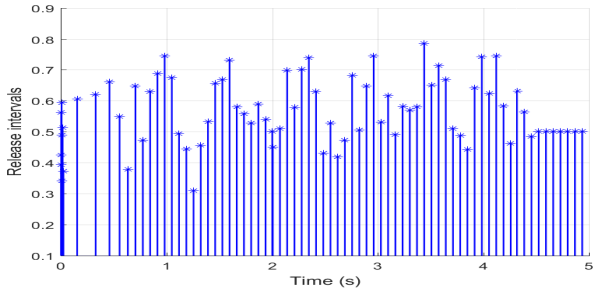

FIGURE 7. Release intervals.

shows that the DETC has a significant impact on the system's control execution. With the minimum value of uncertainties, the control performance is better. Also, the response of the control input is shown in Figure 6. In order to establish the effectiveness of the designed DETC, the state trajectories for the dynamics of different sampling interval values are plotted in Figure 5 by their subsequent gain matrices, which are listed in Table 3. Furthermore, the release instants and

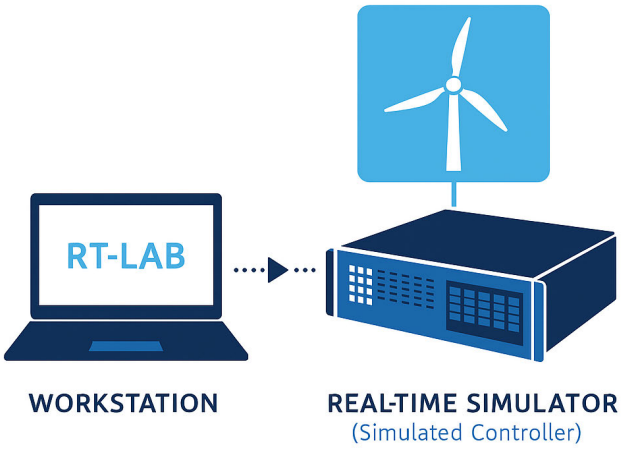

FIGURE 8. Real-time Simulation of proposed system.

release intervals are depicted in Figure 7 with $t \in (0, 15]$. It is clear that implementing the event-triggered mechanism is critical in reducing the frequency of data transfers inside the communication channel while maintaining the wind turbine system's passivity analysis. This strategy improves overall system performance by efficiently eliminating superfluous data exchanges, which adds to the optimal use of network resources. In conclusion, the simulation results demonstrate that the proposed event-triggered controller developed in this study not only stabilizes the target system but also greatly improves communication efficiency by lowering network load. Furthermore, the efficacy and dependability of the established event-triggered mechanism and control technique have been completely confirmed by an extensive study.

VI. REAL-TIME SIMULATION OF PROPOSED SYSTEM

Software-in-the-loop (SIL) simulation helps the real-time simulation of mathematical models in a virtual environment for testing of complex control systems as shown in Figure 8. In this simulation model, the control system interacts directly with the digital plant model running on the OPAL-RT real-time simulation platform enabling rapid prototyping.

To check the feasibility of the proposed model, a MATLAB model of the PMSG with a closed-loop control system is developed as shown in Figure 9. The wind energy conversion system modelling is based on the first principles utilized in this work. The top-level model is presented with the wind speeds as the system input, grid-injected voltage as the system output, and the gate pulses to the power electronic converters as the control input, as shown in the model. This system has two back-to-back connected converters; the first converter is the generator-side converter, and the second is the grid-side converter. Both of these power converters utilize a standard six-switch topology and require gating pulses with pulse width modulation. Both power converters can provide a path for bidirectional power flow from the PMSG to the grid and vice versa.

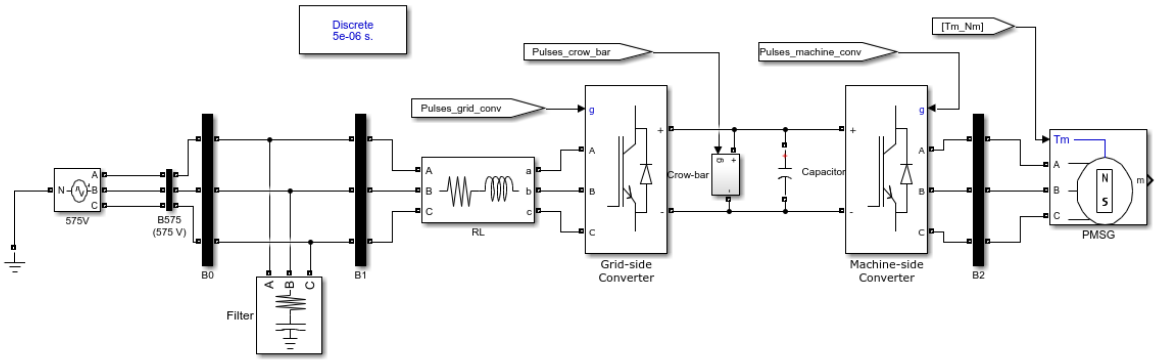

FIGURE 9. Simulation model of the PMSG.

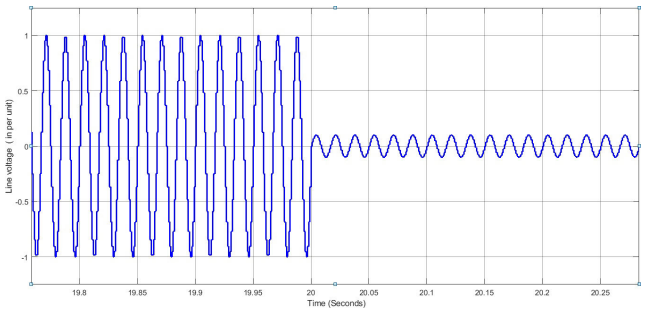

FIGURE 10. Line voltage variation for load step change.

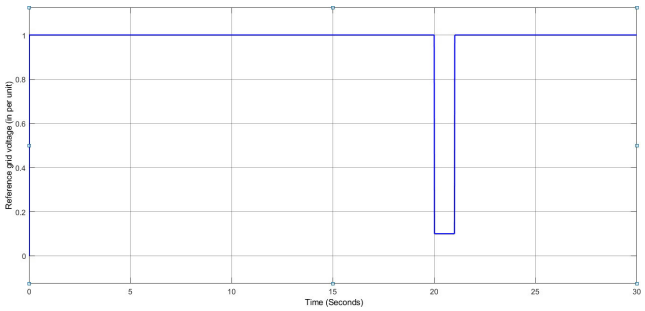

FIGURE 11. Variation in grid reference(in per unit).

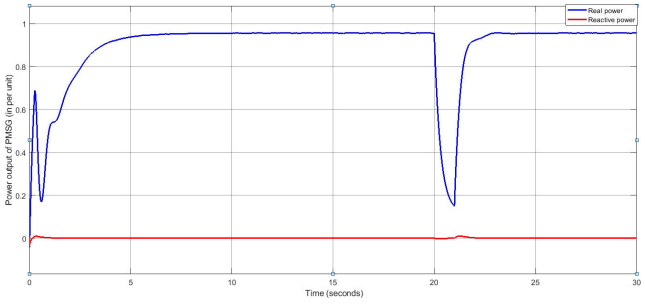

FIGURE 12. Real and reactive power output of the PMSG.

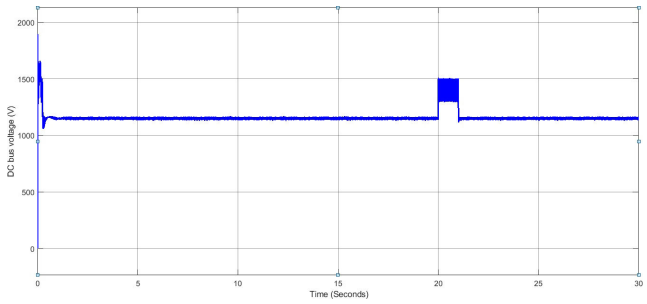

FIGURE 13. DC bus voltage.

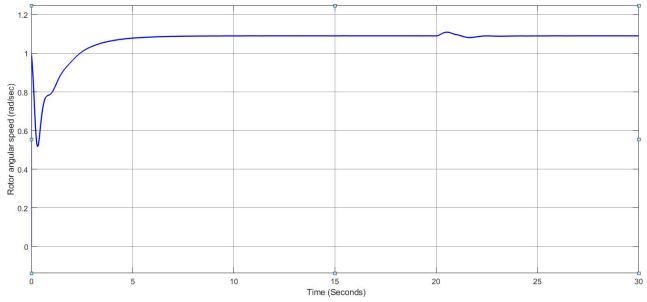

FIGURE 14. Angular speed of the turbine.

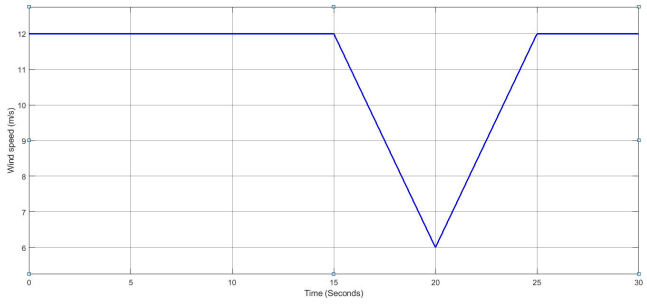

FIGURE 15. Wind speed profile.

A DC bus capacitor is located between the power terminals, which connect the back-to-back power converters. For power exchange, the grid-side converter's output is integrated into the utility grid. The DETC system collects system variables' values from the PMSG, DC bus, and the grid side. Based on the status of different system variables, the centralized control

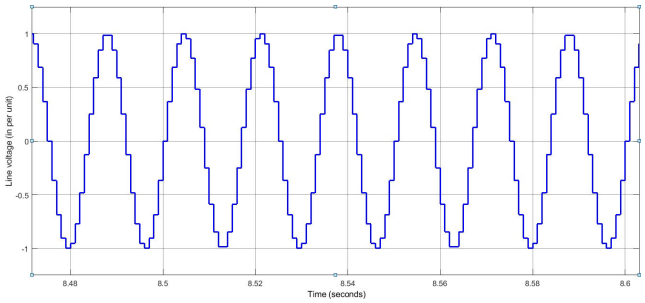

FIGURE 16. Line voltage variation for change in windspeed.

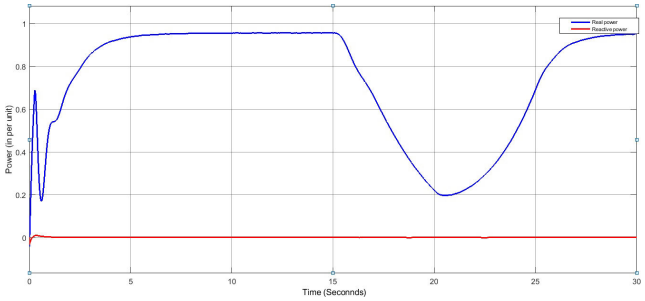

FIGURE 17. Real and reactive power output of the PMSG with windspeed variation.

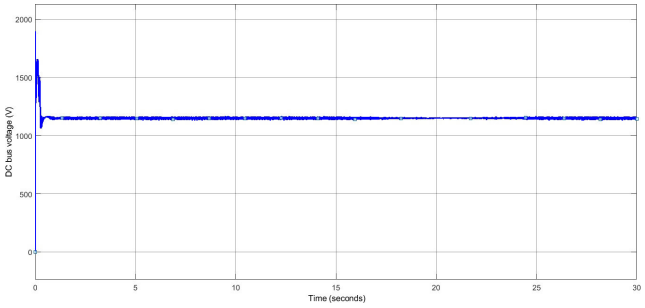

FIGURE 18. DC bus voltage for speed variation.

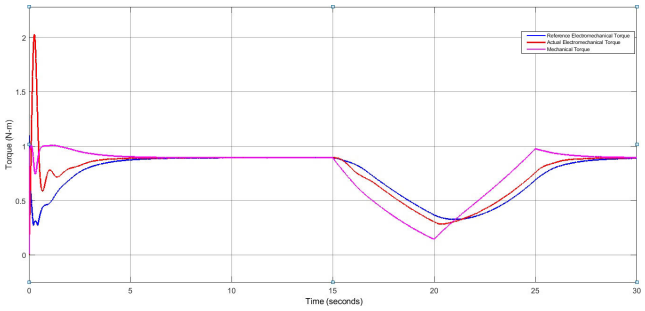

FIGURE 19. Different torque profiles for windspeed variation.

system will modify the control pulses to ensure appropriate three-phase voltage injection to the grid. The wind speed can be modified by changing the input to the PMSG.

A. EFFECT OF VARIATIONS IN THE REFERENCE VOLTAGE

Initially, the system is made to run in a steady state with a fixed wind speed. The PMSG and back-to-back connected

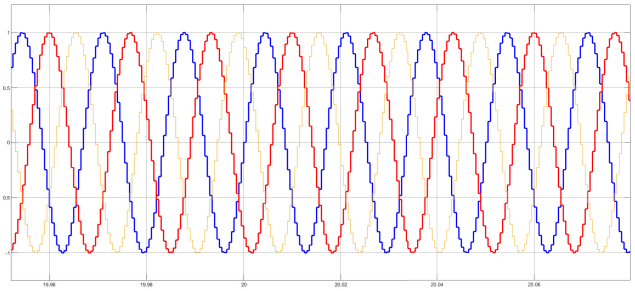

FIGURE 20. Grid injected voltage at point of common coupling.

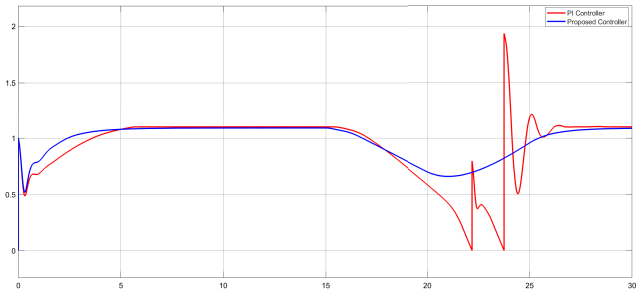

FIGURE 21. Comparison of shaft speed for PI controller and proposed controller.

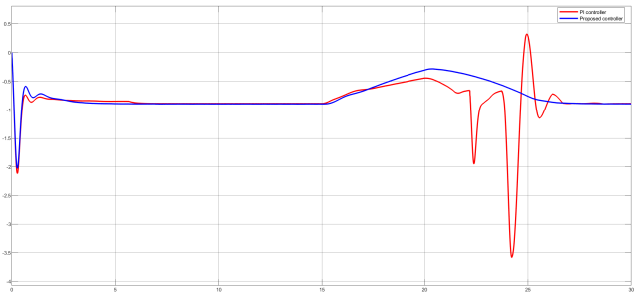

FIGURE 22. Comparison of electromagnetic torque for PI controller and proposed controller.

power converter system are expected to supply power to the grid at prefixed voltage levels. The steady-state system performance is observed. Later, the system is subject to a step variation in the reference voltage injected into the grid. All the voltage levels are considered in the per-unit system. The grid reference voltage suddenly dropped from 1 per unit to 0.1 per unit, and the system response was observed.

The proposed DETC effectively modifies the control variables according to the changes in the reference values. The step variation of the reference voltage in the per-unit system is shown in Figure 11. The variation in the line voltage for the step variation in the reference values are shown in Figure 10. The real and reactive power output of the PMSG also changes according to the variation in the power output of the PMSG as shown in Figure 12, and the same is reflected in the DC bus voltage as shown in Figure 13. The angular speed of the PMSG is shown in Figure 14.

B. EFFECT OF VARIATIONS IN THE WIND SPEED

In the second experiment, the constant wind speed is changed to observe the performance of the proposed system. The wind speed is modified from a constant value of 12 meters per second to a quick variation in the wind speed for a certain period. The wind speed profile is shown in Figure 15. At time t = 15 seconds, the wind speed drops gradually to 6 meters per second and rebounds to 12 meters per second at t = 25 seconds. The purpose of the second experiment is to evaluate the suggested system's performance using different input settings. As the wind speed transforms, the rotor angular speed is also modified, as shown in Figure 18. The sudden drop in the wind speed leads to a drop in the real power output of the PMSG. While the real power output of the PMSG changes, the reactive power output of the generator stays almost constant, as shown in Figure 17.

Point of Common Coupling (PCC) is the location where the transaction between the utility and the customer electrical system takes place. At PCC, the line voltage variation is captured for all three phases when the input wind speed is made to drop as captured in Figure 20. The ramp variation in the wind speed does not have an impact on the voltage injected to the grid.

Even though the wind speed varies, the reference output voltage set by the closed-loop controller is kept constant. The effect of wind speed variation has a minimal impact observed in the constant output line voltage of the PMSG, as shown in Figure 16. The constant output reference voltage of the PMSG directly impacts the electromechanical torque output of the PMSG, as shown in Figure 19. As a result of tests, the DC bus voltage has a minimal impact due to the change in wind speed, as shown in Figure 18. one must note that the presence of an energy storage device on the DC bus has a direct impact on the voltage profile of the DC bus. The transient variations might have a smaller impact on the DC bus voltage, but steady-state variations in wind speed will change the DC bus voltage. Such DC bus voltage changes may lead to a transform in the output voltage to be injected into the grid. In such cases, additional storage devices should complement the DC bus power in steady-state wind speed variations. To establish the feasibility of the proposed control method, a few relevant results of the proposed controller were compared against the PI controller. Two different metrics were considered to compare the performance of the proposed controller and the PI controller. For the given wind speed variation profile, the regulation of shaft speed is compared in the Figure 21. While the steady-state performance is almost similar, the proposed control method exhibits better performance during the transient duration. Similarly, the electromagnetic torque is also considered for comparison, as presented in the Figure 22. As established earlier, the proposed controller is suitable for handling transient variations in the wind profile.

The influence of delay on the proposed model of this paper has stability in typical wind energy conversion systems is presented in Figure 3. It is evident that the presence of a time delay could push the system into unstable conditions. Instead of several delay compensation methods presented in the literature, the proposed system imbibes delay compensation as part of the closed-loop controller without any additional passive components. The event-triggered control mechanism effectively handles transient changes in the reference grid voltage without compensating the system's stability induced by time delay. This is evident from the release intervals presented in Figure 7. Hence, the proposed event-triggered control is effective against both line and load variations.

Remark 15: The wind turbine model studied in this paper differs significantly from existing works in several aspects. How to model the event-triggered scheme of wind turbine system with respect to passivity performance has become one of the main theme in our research work. More particularly, some pioneering works have been done in event-triggered control for PMSG model. Unlike conventional models that rely on periodic control schemes [2], [3], and [8], we propose a decentralized event-triggered control (DETC) framework that reduces communication load by allowing each node to transmit data only when necessary, based on a locally computed condition. Furthermore, the model accounts for interval time-varying delays and actuator uncertainties, which are often neglected in prior studies [5] and [12]. The controller is designed to be non-fragile, enhancing robustness against gain perturbations, an improvement over traditional designs assuming ideal actuators [9] and [16]. A standardized LKF is developed to establish delay-dependent passivity, using relaxed integral inequalities for reduced conservatism, which can induce tighter information on the delay of the considered system. Henceforth, the investigation procedure and framework model proposed in this paper merit a lot of regard for fill such a demand all the more successfully. Overall, our model provides a more realistic and robust framework for modern wind turbine systems operating in communication-constrained environments.

VII. CONCLUSION

In this study, we attempted a unique setup of passivity and passification for the PMSG model using a DDA and DETC. The proposed DETC mechanism aims to reduce unnecessary transmissions and conserve communication bandwidth resources. By creating an appropriate LKF and using special inequality techniques, the passivity execution requirements are produced with regards to LMIs. As a result, DETC has been applied to design the PMSG model and guarantee passivity, and the related gain matrices are obtained. Numerical simulations are presented to demonstrate the effectiveness of the proposed method. The model's behavior and its contribution to the PMSG-WECS stability are covered in the computer simulation studies. Future research could investigate the extension of the proposed conclusions to the presence of adaptive event-triggered control under fault effects in the PMSG model. In real-world scenarios, the

articulated design may help create more robust and effective control techniques for PMSG-based wind energy conversion systems, which might result in more dependable and effective wind energy conversion systems. In addition, will focus on extending this work to include adaptive or dynamic event-triggered control under various fault effects in PMSG models. A critical next step involves thoroughly exploring the robustness of this decentralized control approach against different uncertainties and disturbances. Practical validation through hardware-in-the-loop (HIL) simulations or experimental prototypes will also be pursued. Finally, the applicability of this passivity-based control strategy to other large-scale distributed energy systems, such as smart grids, warrants further investigation. Also, extending the proposed approach to multi-agent wind energy systems, incorporating stochastic disturbances, exploring adaptive event-triggered strategies under more complex environmental uncertainties. These extensions aim to broaden the applicability and robustness of the proposed framework.

APPENDIX

Theorem 7 LMI terms:

$$\theta_{1,1} = Q_1 + Q_2 + Q_3 + \alpha\delta U_{11} + U_{13} + U_{13}^T + R_1 - \frac{\pi^2}{4}R_3 - 9R_2 - \frac{h_3 - \eta_2(t)}{h_3}9R_2 - 6R_5 + 2L\bar{A}_0,$$
$$\theta_{1,2} = L\bar{A}_1,\ \theta_{1,4} = \alpha\delta U_{12} - U_{13} + U_{23}^T,$$
$$\theta_{1,5} = 3R_2 + \frac{h_3 - \eta_2(t)}{h_3}3R_2 + R_3\frac{\pi^2}{4} + L\bar{B}\tilde{K},$$
$$\theta_{1,7} = -24R_2 - \frac{h_3 - \eta_2(t)}{h_3}24R_2,$$
$$\theta_{1,8} = 60R_2 + \frac{h_3 - \eta_2(t)}{h_3}60R_2,$$
$$\theta_{1,11} = P - L + (L\bar{A}_0)^T,\ \theta_{1,12} = -L\bar{B}\tilde{K},$$
$$\theta_{1,13} = -6R_5,\ \theta_{1,14} = 24R_5,$$
$$\theta_{2,2} = -(1-h_d)Q_3 + (d_2 - \alpha\delta)V_{22} - V_{23} - V_{23}^T + (d_2 - \alpha\delta)W_{11} + W_{13} + W_{13}^T,\ \theta_{1,17} = L\bar{A}_2 - I,$$
$$\theta_{2,3} = (d_2 - \alpha\delta)W_{12} - W_{13} + W_{23}^T,$$
$$\theta_{2,4} = (d_2 - \alpha\delta)V_{12}^T - V_{13}^T + V_{23},\ \theta_{2,11} = (L\bar{A}_1)^T$$
$$\theta_{3,3} = -Q_2 - 6R_6 + (d_2 - \alpha\delta)W_{22} - W_{23} - W_{23}^T,$$
$$\theta_{3,15} = 18R_6,\ \theta_{3,16} = -24R_6,$$
$$\theta_{4,4} = -Q_1 - 6R_4 - 6R_7 + (d_2 - \alpha\delta)V_{11} + V_{13} + V_{13}^T + \alpha\delta U_{22} - U_{23} - U_{23}^T,\ \theta_{4,13} = 18R_4,$$
$$\theta_{4,14} = -24R_4,\ \theta_{4,15} = -6R_7,\ \theta_{4,16} = 24R_7$$
$$\theta_{5,5} = -18R_2 - \frac{h_3 - \eta_2(t)}{h_3}9R_2 - \frac{\eta_2(t)}{h_3}9R_2 - \frac{\pi^2}{4}R_3 + \sigma\phi,\ \theta_{5,6} = 3R_2 + (\frac{\eta_2(t)}{h_3})3R_2,$$
$$\theta_{5,7} = 36R_2 + (\frac{h_3 - \eta_2(t)}{h_3})36R_2,\ \theta_{5,8} = -60R_2 - \frac{h_3 - \eta_2(t)}{h_3}60R_2,\ \theta_{5,9} = 6R_2 + (\frac{\eta_2(t)}{h_3})6R_2,$$
$$\theta_{5,10} = 60R_2 + \frac{\eta_2(t)}{h_3}60R_2,\ \theta_{5,11} = (L\bar{B}\tilde{K})^T,$$
$$\theta_{6,6} = -9R_2 - \frac{\eta_2(t)}{h_3}9R_2,\ \theta_{6,9} = 6R_2 + \frac{\eta_2(t)}{h_3}6R_2,$$
$$\theta_{6,10} = -60R_2 - \frac{\eta_2(t)}{h_3}60R_2,\ \theta_{7,7} = -192R_2 - \frac{h_3 - \eta_2(t)}{h_3}(192R_2),\ \theta_{5,12} = -\sigma\phi,\ \theta_{7,8} = 360R_2 + \frac{h_3 - \eta_2(t)}{h_3}360R_2,\ \theta_{8,8} = -720R_2 - \frac{h_3 - \eta_2(t)}{h_3}720R_2,\ \theta_{9,9} = -12R_2 - \frac{\eta_2(t)}{h_3}12R_2,$$
$$\theta_{10,10} = -720R_2 - \frac{\eta_2(t)}{h_3}720R_2,\ \theta_{11,11} = Q_4\alpha\delta + Q_5(d_2 - \alpha\delta) + h_3^2R_2 + h_3^2R_3 + \frac{(\alpha\delta)^2}{2}(R_4 + R_5) + \frac{(d_2 - \alpha\delta)^2}{2}(R_6 + R_7) - 2L,\ \theta_{11,12} = -L\bar{B}\tilde{K},$$
$$\theta_{11,17} = L\bar{A}_2,\ \theta_{12,12} = -(1-\sigma)\phi,\ \theta_{13,13} = -66R_4 - 18R_5,$$
$$\theta_{13,14} = 96R_4 + 48R_5,\ \theta_{14,14} = -144R_4 - 144R_5,$$
$$\theta_{15,15} = -66R_6 - 18R_7,\ \theta_{15,16} = 96R_6 + 48R_7,$$
$$\theta_{16,16} = -144R_6 - 144R_7,\ \theta_{17,17} = -\gamma I.$$

Moreover, Theorem 10 LMI terms

$$\hat{\theta}_{1,1} = Q_1 + Q_2 + Q_3 + \alpha\delta U_{11} + U_{13} + U_{13}^T + R_1 - \frac{\pi^2}{4}R_3 - 9R_2 - \frac{h_3 - \eta_2(t)}{h_3}9R_2 - 6R_5 + 2LA_0,$$
$$\hat{\theta}_{1,2} = LA_1,\ \hat{\theta}_{1,4} = \alpha\delta U_{12} - U_{13} + U_{23}^T,$$
$$\hat{\theta}_{1,5} = 3R_2 + \frac{h_3 - \eta_2(t)}{h_3}3R_2 + R_3\frac{\pi^2}{4} + LBK,$$
$$\hat{\theta}_{1,7} = -24R_2 - \frac{h_3 - \eta_2(t)}{h_3}24R_2,$$
$$\hat{\theta}_{1,8} = 60R_2 + \frac{h_3 - \eta_2(t)}{h_3}60R_2,$$
$$\hat{\theta}_{1,11} = P - L + (LA_0)^T,\ \hat{\theta}_{1,12} = -LBK,$$
$$\hat{\theta}_{1,13} = -6R_5,\ \hat{\theta}_{1,14} = 24R_5,$$
$$\hat{\theta}_{2,2} = -(1-h_d)Q_3 + (d_2 - \alpha\delta)V_{22} - V_{23} - V_{23}^T + (d_2 - \alpha\delta)W_{11} + W_{13} + W_{13}^T,\ \hat{\theta}_{1,17} = L\bar{A}_2 - I,$$
$$\hat{\theta}_{2,3} = (d_2 - \alpha\delta)W_{12} - W_{13} + W_{23}^T,$$
$$\hat{\theta}_{2,4} = (d_2 - \alpha\delta)V_{12}^T - V_{13}^T + V_{23},\ \hat{\theta}_{2,11} = (LA_1)^T,$$
$$\hat{\theta}_{3,3} = -Q_2 - 6R_6 + (d_2 - \alpha\delta)W_{22} - W_{23} - W_{23}^T,$$
$$\hat{\theta}_{3,15} = 18R_6,\ \hat{\theta}_{3,16} = -24R_6,$$
$$\hat{\theta}_{4,4} = -Q_1 - 6R_4 - 6R_7 + (d_2 - \alpha\delta)V_{11} + V_{13} + V_{13}^T + \alpha\delta U_{22} - U_{23} - U_{23}^T,\ \hat{\theta}_{4,13} = 18R_4,$$
$$\hat{\theta}_{4,14} = -24R_4,\ \hat{\theta}_{4,15} = -6R_7,\ \hat{\theta}_{4,16} = 24R_7,$$
$$\hat{\theta}_{5,5} = -18R_2 - \frac{h_3 - \eta_2(t)}{h_3}9R_2 - \frac{\eta_2(t)}{h_3}9R_2$$

$$-\frac{\pi^2}{4}R_3+\sigma\phi,\ \hat{\theta}_{5,6}=3R_2+(\frac{\eta_2(t)}{h_3})3R_2,$$
$$\hat{\theta}_{5,7}=36R_2+(\frac{h_3-\eta_2(t)}{h_3})36R_2,\ \hat{\theta}_{5,8}=-60R_2,$$
$$-\frac{h_3-\eta_2(t)}{h_3}60R_2,\ \hat{\theta}_{5,9}=6R_2+(\frac{\eta_2(t)}{h_3})6R_2,$$
$$\hat{\theta}_{5,10}=60R_2+\frac{\eta_2(t)}{h_3}60R_2,\ \hat{\theta}_{5,11}=(LBK)^T,$$
$$\hat{\theta}_{6,6}=-9R_2-\frac{\eta_2(t)}{h_3}9R_2,\ \hat{\theta}_{6,9}=6R_2+\frac{\eta_2(t)}{h_3}6R_2,$$
$$\hat{\theta}_{6,10}=-60R_2-\frac{\eta_2(t)}{h_3}60R_2,\ \hat{\theta}_{7,7}=-192R_2$$
$$-\frac{h_3-\eta_2(t)}{h_3}(192R_2),\ \hat{\theta}_{5,12}=-\sigma\phi,\ \hat{\theta}_{7,8}=360R_2$$
$$+\frac{h_3-\eta_2(t)}{h_3}360R_2,\ \hat{\theta}_{8,8}=-720R_2$$
$$-\frac{h_3-\eta_2(t)}{h_3}720R_2,\ \hat{\theta}_{9,9}=-12R_2-\frac{\eta_2(t)}{h_3}12R_2,$$
$$\hat{\theta}_{10,10}=-720R_2-\frac{\eta_2(t)}{h_3}720R_2,$$
$$\hat{\theta}_{11,11}=Q_4\alpha\delta+Q_5(d_2-\alpha\delta)$$
$$+h_3^2R_2+h_3^2R_3+\frac{(\alpha\delta)^2}{2}(R_4+R_5)$$
$$+\frac{(d_2-\alpha\delta)^2}{2}(R_6+R_7)-2L,\ \hat{\theta}_{11,12}=-LBK,$$
$$\hat{\theta}_{11,17}=L\bar{A}_2,\ \hat{\theta}_{12,12}=-(1-\sigma)\phi,\ \hat{\theta}_{13,13}=-66R_4-18R_5,$$
$$\hat{\theta}_{13,14}=96R_4+48R_5,\ \hat{\theta}_{14,14}=-144R_4-144R_5,$$
$$\hat{\theta}_{15,15}=-66R_6-18R_7,\ \hat{\theta}_{15,16}=96R_6+48R_7,$$
$$\hat{\theta}_{16,16}=-144R_6-144R_7,\ \hat{\theta}_{17,17}=-\gamma I,$$
$$\Gamma_3=[\mathcal{E}_0^TB^TL^T\ \underbrace{0,\cdots,0}_{9\ times}\ \mathcal{E}_0^TB^TL^T\ \underbrace{0,\cdots,0}_{7\ times}\ \mathcal{E}_0^TH_3^T]^T,$$
$$\Gamma_4=[\underbrace{0,\cdots,0}_{4\ times}\ \mathcal{E}_1K\ \underbrace{0,\cdots,0}_{6\ times}\ -\mathcal{E}_1K\ \underbrace{0,\cdots,0}_{7\ times}].$$

Theorem 10 LMI terms

$$\hat{\Psi}_{1,1}=\hat{Q}_1+\hat{Q}_2+\hat{Q}_3+\alpha\delta\hat{U}_{11}+2\hat{U}_{13}+\hat{R}_1-\frac{\pi^2}{4}\hat{R}_3$$
$$-9\hat{R}_2-\frac{h_3-\eta_2(t)}{h_3}9\hat{R}_2-6\hat{R}_5+2A_0\mathcal{X},$$
$$\hat{\Psi}_{1,2}=A_1\mathcal{X},\ \hat{\Psi}_{1,4}=\alpha\delta\hat{U}_{12}-\hat{U}_{13}+\hat{U}_{23}^T,$$
$$\hat{\Psi}_{1,5}=3\hat{R}_2+\frac{h_3-\eta_2(t)}{h_3}3\hat{R}_2+\hat{R}_3\frac{\pi^2}{4}+BY,$$
$$\hat{\Psi}_{1,7}=-24\hat{R}_2-\frac{h_3-\eta_2(t)}{h_3}24\hat{R}_2,$$
$$\hat{\Psi}_{1,8}=60\hat{R}_2+\frac{h_3-\eta_2(t)}{h_3}60\hat{R}_2,\ \hat{\Psi}_{1,11}=\mathcal{X}A_0^T,$$
$$\hat{\Psi}_{1,12}=-BY,\ \hat{\Psi}_{1,13}=-6\hat{R}_5,\ \hat{\Psi}_{1,14}=24\hat{R}_5,$$
$$\hat{\Psi}_{1,17}=\bar{A}_2-\mathcal{X},\ \hat{\Psi}_{1,18}=\mathcal{G},\ \hat{\Psi}_{1,19}=\mathcal{X}\mathcal{H}_1^T,$$
$$\hat{\Psi}_{1,20}=B\mathcal{E}_0,\ \hat{\Psi}_{2,2}=-(1-h_d)\hat{Q}_3+(d_2-\alpha\delta)\hat{V}_{22}$$
$$-\hat{V}_{23}-\hat{V}_{23}^T+(h_2-\alpha\delta)\hat{W}_{11}+2\hat{W}_{13},$$
$$\hat{\Psi}_{2,3}=(d_2-\alpha\delta)\hat{W}_{12}-\hat{W}_{13}+\hat{W}_{23}^T,$$
$$\hat{\Psi}_{2,4}=(d_2-\alpha\delta)\hat{V}_{12}^T-\hat{V}_{13}^T+\hat{V}_{23},$$
$$\hat{\Psi}_{2,11}=\mathcal{X}A_1^T,\ \hat{\Psi}_{2,19}=\mathcal{X}\mathcal{H}_2^T,$$
$$\hat{\Psi}_{3,3}=-\hat{Q}_2-6\hat{R}_6+(d_2-\alpha\delta)\hat{W}_{22}-\hat{W}_{23}-\hat{W}_{23}^T,$$
$$\hat{\Psi}_{3,15}=18\hat{R}_6,\ \hat{\Psi}_{3,16}=-24\hat{R}_6$$
$$\hat{\Psi}_{4,4}=-\hat{Q}_1-6\hat{R}_4-6\hat{R}_7+(d_2-\alpha\delta)\hat{V}_{11}+2\hat{V}_{13}$$
$$+\alpha\delta\hat{U}_{22}-2\hat{U}_{23},$$
$$\hat{\Psi}_{4,13}=18\hat{R}_4,\ \hat{\Psi}_{4,14}=-24\hat{R}_4,\ \hat{\Psi}_{4,15}=-6\hat{R}_7,$$
$$\hat{\Psi}_{4,16}=24\hat{R}_7,\ \hat{\Psi}_{5,5}=-9\hat{R}_2\big(2+\frac{h_3-\eta_2(t)}{h_3}+\frac{\eta_2(t)}{h_3}\big)$$
$$-\frac{\pi^2}{4}\hat{R}_3+\sigma\hat{\phi},\ \hat{\Psi}_{5,6}=3\hat{R}_2+\frac{\eta_2(t)}{h_3}3\hat{R}_2,$$
$$\hat{\Psi}_{5,7}=36\hat{R}_2+\frac{h_3-\eta_2(t)}{h_3}36\hat{R}_2,\ \hat{\Psi}_{5,8}=-60\hat{R}_2$$
$$-\frac{h_3-\eta_2(t)}{h_3}60\hat{R}_2,\ \hat{\Psi}_{5,9}=6\hat{R}_2+\frac{\eta_2(t)}{h_3}6\hat{R}_2,$$
$$\hat{\Psi}_{5,10}=60\hat{R}_2+\frac{\eta_2(t)}{h_3}60\hat{R}_2,\ \hat{\Psi}_{5,11}=Y^TB^T,$$
$$\hat{\Psi}_{5,19}=Y^T\mathcal{H}_3^T,\ \hat{\Psi}_{5,21}=Y^T\mathcal{E}_1^T,$$
$$\hat{\Psi}_{6,6}=-9\hat{R}_2-\frac{\eta_2(t)}{h_3}9\hat{R}_2,\ \hat{\Psi}_{6,9}=6\hat{R}_2+\frac{\eta_2(t)}{h_3}6\hat{R}_2,$$
$$\hat{\Psi}_{6,10}=-60\hat{R}_2-\frac{\eta_2(t)}{h_3}60\hat{R}_2,\ \hat{\Psi}_{5,12}=-\sigma\hat{\phi},$$
$$\hat{\Psi}_{7,7}=-192\hat{R}_2\big(1+\frac{h_3-\eta_2(t)}{h_3}\big),\ \hat{\Psi}_{7,8}=360\hat{R}_2\big(1$$
$$+\frac{h_3-\eta_2(t)}{h_3}\big),\ \hat{\Psi}_{8,8}=-720\hat{R}_2\big(1-\frac{h_3-\eta_2(t)}{h_3}\big),$$
$$\hat{\Psi}_{9,9}=-12\hat{R}_2-\frac{\eta_2(t)}{h_3}12\hat{R}_2,$$
$$\hat{\Psi}_{10,10}=-720\hat{R}_2-\frac{\eta_2(t)}{h_3}720\hat{R}_2,\ \hat{\Psi}_{11,11}=\hat{Q}_4\alpha\delta$$
$$+\hat{Q}_5(d_2-\alpha\delta)+h_3^2(\hat{R}_2+\hat{R}_3)+\frac{(\alpha\delta)^2}{2}(\hat{R}_4+\hat{R}_5)$$
$$+\frac{(d_2-\alpha\delta)^2}{2}(\hat{R}_6+\hat{R}_7)-2\mathcal{X},\ \hat{\Psi}_{11,12}=-BY,$$
$$\hat{\Psi}_{11,17}=\bar{A}_2,\ \hat{\Psi}_{11,18}=\mathcal{G},\ \hat{\Psi}_{11,20}=B\mathcal{E}_0,$$
$$\hat{\Psi}_{12,12}=-(1-\sigma)\hat{\phi},\ \hat{\Psi}_{12,19}=-Y^T\mathcal{H}_3^T,$$
$$\hat{\Psi}_{19,20}=H_3\mathcal{E}_0,\ \hat{\Psi}_{12,21}=-Y^T\mathcal{E}_1^T,$$
$$\hat{\Psi}_{13,13}=-66\hat{R}_4-18\hat{R}_5,\ \hat{\Psi}_{13,14}=96\hat{R}_4+48\hat{R}_5,$$
$$\hat{\Psi}_{14,14}=-144\hat{R}_4-144\hat{R}_5,\ \hat{\Psi}_{15,15}=-66\hat{R}_6-18\hat{R}_7,$$
$$\hat{\Psi}_{15,16}=96\hat{R}_6+48\hat{R}_7,\ \hat{\Psi}_{16,16}=-144\hat{R}_6-144\hat{R}_7,$$
$$\hat{\Psi}_{17,17}=-\gamma I,\ \hat{\Psi}_{18,18}=-\epsilon_1 I,\ \hat{\Psi}_{19,19}=-\epsilon_1^{-1}I,$$
$$\hat{\Psi}_{20,20}=-\epsilon_2 I,\ \hat{\Psi}_{21,21}=-\epsilon_2^{-1}I,$$

REFERENCES

[1] M. Cheng and Y. Zhu, "The state of the art of wind energy conversion systems and technologies: A review," *Energy Convers. Manage.*, vol. 88, pp. 332–347, Dec. 2014.

[2] A. G. Sanchez, M. G. Molina, and A. M. R. Lede, "Dynamic model of wind energy conversion systems with PMSG-based variable-speed wind turbines for power system studies," *Int. J. Hydrogen Energy*, vol. 37, no. 13, pp. 10064–10069, Jul. 2012.

[3] S. Sajedi, H. J. Rezabeyglo, A. Noruzi, F. Khalifeh, T. Karimi, and Z. Khalifeh, "Modeling and application of PMSG based variable speed wind generation system," *Res. J. Appl. Sci., Eng. Technol.*, vol. 4, no. 7, pp. 729–734, 2012.

[4] R. Subramaniyam and Y. H. Joo, "Memory-based ISMC design of DFIG-based wind turbine model via T-S fuzzy approach," *IET Control Theory Appl.*, vol. 15, no. 3, pp. 348–359, Feb. 2021.

[5] P. Mani and Y. H. Joo, "Fuzzy event-triggered control for back-to-back converter involved PMSG-based wind turbine systems," *IEEE Trans. Fuzzy Syst.*, vol. 30, no. 5, pp. 1409–1420, May 2022.

[6] M. M. R. Singaravel and S. A. Daniel, "MPPT with single DC–DC converter and inverter for grid-connected hybrid wind-driven PMSG–PV system," *IEEE Trans. Ind. Electron.*, vol. 62, no. 8, pp. 4849–4857, Aug. 2015.

[7] G. Hangaragi, "DC–DC converter and inverter for grid connected hybrid wind-driven PMSG-PV system with MPPT," *Indian J. Sci. Res.*, vol. 2015, pp. 13–21, Nov. 2015.

[8] F. D. Bianchi, R. J. Mantz, and C. F. Christiansen, "Gain scheduling control of variable-speed wind energy conversion systems using quasi-LPV models," *Control Eng. Pract.*, vol. 13, no. 2, pp. 247–255, Feb. 2005.

[9] R. Vadivel and Y. H. Joo, "Reliable fuzzy H_∞ control for permanent magnet synchronous motor against stochastic actuator faults," *IEEE Trans. Syst., Man, Cybern., Syst.*, vol. 51, no. 4, pp. 2232–2245, Apr. 2021.

[10] G. Scorletti and V. Fromion, "A unified approach to time-delay system control: Robust and gain-scheduled," in *Proc. Amer. Control Conf. (ACC)*, vol. 4, Jul. 1998, pp. 2391–2395.

[11] H. C. Sung, J. B. Park, and Y. H. Joo, "Robust observer-based fuzzy control for variable speed wind power system: LMI approach," *Int. J. Control, Autom. Syst.*, vol. 9, no. 6, pp. 1103–1110, Dec. 2011.

[12] R. Saravanakumar and Y. H. Joo, "Fuzzy dissipative and observer control for wind generator systems: A fuzzy time-dependent LKF approach," *Nonlinear Dyn.*, vol. 97, no. 4, pp. 2189–2199, Sep. 2019.

[13] Q. Zhong, J. Yang, K. Shi, S. Zhong, Z. Li, and M. A. Sotelo, "Event-triggered H_∞ load frequency control for multi-area nonlinear power systems based on non-fragile proportional integral control strategy," *IEEE Trans. Intell. Transp. Syst.*, vol. 23, no. 8, pp. 12191–12201, Aug. 2022.

[14] C. Zhang, Y. He, L. Jiang, M. Wu, and H. Zeng, "Stability analysis of systems with time-varying delay via relaxed integral inequalities," *Syst. Control Lett.*, vol. 92, pp. 52–61, May 2016.

[15] L. Shanmugam and Y. H. Joo, "Investigation on stability of delayed T-S fuzzy interconnected systems via decentralized memory-based sampled-data control and validation through interconnected power systems with DFIG-based wind turbines," *Inf. Sci.*, vol. 580, pp. 934–952, Nov. 2021.

[16] X. Cai, J. Wang, K. Shi, S. Zhong, and T. Jiang, "Quantized dissipative control based on T–S fuzzy model for wind generation systems," *ISA Trans.*, vol. 126, pp. 533–544, Jul. 2022.

[17] M. S. Mahmoud, "Passive control synthesis for uncertain time-delay systems," in *Proc. 37th IEEE Conf. Decis. Control*, vol. 4, Aug. 1998, pp. 4139–4143.

[18] C. Li and X. Liao, "Passivity analysis of neural networks with time delay," *IEEE Trans. Circuits Syst. II, Exp. Briefs*, vol. 52, no. 8, pp. 471–475, Aug. 2005.

[19] M. Sathishkumar, R. Sakthivel, O. M. Kwon, and B. Kaviarasan, "Finite-time mixed H_∞ and passive filtering for Takagi–Sugeno fuzzy nonhomogeneous Markovian jump systems," *Int. J. Syst. Sci.*, vol. 48, no. 7, pp. 1416–1427, May 2017.

[20] R. Vadivel and Y. H. Joo, "Finite-time sampled-data fuzzy control for a non-linear system using passivity and passification approaches and its application," *IET Control Theory Appl.*, vol. 14, no. 8, pp. 1033–1045, May 2020.

[21] G. Nagamani, Y. H. Joo, G. Soundararajan, and R. Mohajerpoor, "Robust event-triggered reliable control for T-S fuzzy uncertain systems via weighted based inequality," *Inf. Sci.*, vol. 512, pp. 31–49, Feb. 2020.

[22] R. Vadivel, P. Hammachukiattikul, G. Rajchakit, M. Syed Ali, and B. Unyong, "Finite-time event-triggered approach for recurrent neural networks with leakage term and its application," *Math. Comput. Simul.*, vol. 182, pp. 765–790, Apr. 2021.

[23] M. Shen, Y. Gu, J. H. Park, Y. Yi, and W.-W. Che, "Composite control of linear systems with event-triggered inputs and outputs," *IEEE Trans. Circuits Syst. II, Exp. Briefs*, vol. 69, no. 3, pp. 1154–1158, Mar. 2022.

[24] R. Vadivel, M. S. Ali, and Y. H. Joo, "Drive-response synchronization of uncertain Markov jump generalized neural networks with interval time varying delays via decentralized event-triggered communication scheme," *J. Franklin Inst.*, vol. 357, no. 11, pp. 6824–6857, Jul. 2020.

[25] M. Shen, X. Wang, S. Zhu, Z. Wu, and T. Huang, "Data-driven event-triggered adaptive dynamic programming control for nonlinear systems with input saturation," *IEEE Trans. Cybern.*, vol. 54, no. 2, pp. 1178–1188, Feb. 2024.

[26] X. Wang and M. D. Lemmon, "Event-triggering in distributed networked control systems," *IEEE Trans. Autom. Control*, vol. 56, no. 3, pp. 586–601, Mar. 2011.

[27] P. Tallapragada and N. Chopra, "Event-triggered dynamic output feedback control for LTI systems," in *Proc. IEEE 51st IEEE Conf. Decis. control (CDC)*, Jun. 2012, pp. 6597–6602.

[28] W. P. M. H. Heemels, M. C. F. Donkers, and A. R. Teel, "Periodic event-triggered control for linear systems," *IEEE Trans. Autom. Control*, vol. 58, no. 4, pp. 847–861, Apr. 2013.

[29] J. Zhang and C. Peng, "Synchronization of master–slave neural networks with a decentralized event triggered communication scheme," *Neurocomputing*, vol. 173, pp. 1824–1831, Jan. 2016.

[30] S. Kartakis, A. Fu, M. Mazo, and J. A. McCann, "Communication schemes for centralized and decentralized event-triggered control systems," *IEEE Trans. Control Syst. Technol.*, vol. 26, no. 6, pp. 2035–2048, Nov. 2018.

[31] R. Subramaniam and Y. H. Joo, "Passivity-based fuzzy ISMC for wind energy conversion systems with PMSG," *IEEE Trans. Syst., Man, Cybern., Syst.*, vol. 51, no. 4, pp. 2212–2220, Apr. 2021.

[32] M. J. Alden and X. Wang, "Robust H_∞ control of time delayed power systems," *Syst. Sci. Control Eng.*, vol. 3, no. 1, pp. 253–261, 2015.

[33] S. Buso and P. Mattavelli, *Digital Control in Power Electronics*. Cham, Switzerland: Springer, 2022.

[34] C. Zou, B. Liu, S. Duan, and R. Li, "Influence of delay on system stability and delay optimization of grid-connected inverters with LCL filter," *IEEE Trans. Ind. Informat.*, vol. 10, no. 3, pp. 1775–1784, Aug. 2014.

[35] T. Zhao, J. Li, and N. Gao, "Capacitor-current-feedback with improved delay compensation for LCL-type grid-connected inverter to achieve high robustness in weak grid," *IEEE Access*, vol. 10, pp. 127956–127968, 2022.

[36] H. Bevrani and T. Hiyama, "Robust decentralised PI based LFC design for time delay power systems," *Energy Convers. Manage.*, vol. 49, no. 2, pp. 193–204, Feb. 2008.

[37] W. Yao, L. Jiang, Q. H. Wu, J. Y. Wen, and S. J. Cheng, "Delay-dependent stability analysis of the power system with a wide-area damping controller embedded," *IEEE Trans. Power Syst.*, vol. 26, no. 1, pp. 233–240, Feb. 2011.

[38] M. S. Ali, N. Gunasekaran, and R. Saravanakumar, "Design of passivity and passification for delayed neural networks with Markovian jump parameters via non-uniform sampled-data control," *Neural Comput. Appl.*, vol. 30, no. 2, pp. 595–605, Jul. 2018.

[39] J.-A. Wang, X.-Y. Wen, and B.-Y. Hou, "Advanced stability criteria for static neural networks with interval time-varying delays via the improved Jensen inequality," *Neurocomputing*, vol. 377, pp. 49–56, Feb. 2020.

[40] P.-L. Liu, "Improved delay-range-dependent robust stability for uncertain systems with interval time-varying delay," *ISA Trans.*, vol. 53, no. 6, pp. 1731–1738, Nov. 2014.

[41] R. Sakthivel, T. Saravanakumar, Y.-K. Ma, and S. Marshal Anthoni, "Finite-time resilient reliable sampled-data control for fuzzy systems with randomly occurring uncertainties," *Fuzzy Sets Syst.*, vol. 329, pp. 1–18, Dec. 2017.

[42] S. He, "Non-fragile passive controller design for nonlinear Markovian jumping systems via observer-based controls," *Neurocomputing*, vol. 147, pp. 350–357, Jan. 2015.

[43] H. Gao and T. Chen, "Stabilization of nonlinear systems under variable sampling: A fuzzy control approach," *IEEE Trans. Fuzzy Syst.*, vol. 15, no. 5, pp. 972–983, Oct. 2007.

[44] B. Yang, T. Yu, H. Shu, Y. Zhang, J. Chen, Y. Sang, and L. Jiang, "Passivity-based sliding-mode control design for optimal power extraction of a PMSG based variable speed wind turbine," *Renew. Energy*, vol. 119, pp. 577–589, Apr. 2018.

[45] B. Yang, T. Yu, H. Shu, D. Qiu, Y. Zhang, P. Cao, and L. Jiang, "Passivity-based linear feedback control of permanent magnetic synchronous generator-based wind energy conversion system: Design and analysis," *IET Renew. Power Gener.*, vol. 12, no. 9, pp. 981–991, Jul. 2018.
[46] A. Monroy, L. Alvarez-Icaza, and G. Espinosa-Pérez, "Passivity-based control for variable speed constant frequency operation of a DFIG wind turbine," *Int. J. Control*, vol. 81, no. 9, pp. 1399–1407, Sep. 2008.

R. VADIVEL received the B.Sc., M.Sc., M.Phil. degrees in mathematics from the Sri Ramakrishna Mission Vidyalaya College of Arts and Science, Bharathiar University, Tamil Nadu, India, and the Ph.D. degree in mathematics from the Department of Mathematics, Thiruvalluvar University, India. He was a Postdoctoral Research Fellow with the Research Center for Wind Energy Systems, Kunsan National University, Gunsan, South Korea, from 2018 to 2019. He is currently a Lecturer with the Department of Mathematics, Faculty of Science and Technology, Phuket Rajabhat University, Thailand. He has authored and co-authored more than 60 research articles in various SCI journals. His research interests include control theory, stability analysis, event-triggered control, networked control systems, neural networks, and T-S fuzzy theory. He serves as a reviewer for various SCI journals.

T. K. SANTHOSH received the B.E. degree in electrical and electronics engineering from the Kumaraguru College of Technology, Coimbatore, India, in 2009, and the M.E. degree in power electronics and drives from the K.S.R. College of Engineering, Tiruchengode, India, in 2011. After a short academic stint, he was selected to pursue his full-time Ph.D. degree in electrical engineering under Anna University, Chennai. During the Ph.D. degree, he was a Teaching Research Associate with the Department of Electrical and Electronics Engineering, Government College of Engineering, Salem. He is currently heading the Electric Vehicle Research Group, SASTRA Deemed University, Tamil Nadu, India, where he is a Senior Assistant Professor with the School of Electrical and Electronics Engineering.

R. SURESH received the M.Sc., M.Phil., and Ph.D. degrees in mathematics from Bharathiar University, Coimbatore, Tamil Nadu, India, in 2007, 2010, and 2017, respectively. He is currently an Assistant Professor with the Department of Applied Mathematics, Sri Venkateswara College of Engineering, Sriperumbudur, Tamil Nadu. His current research interests include control theory and its applications for linear and nonlinear systems, time delay systems, neural networks, and stochastic systems.

NALLAPPAN GUNASEKARAN received the Ph.D. degree in mathematics from Thiruvalluvar University, Vellore, India, in 2018. He was a Junior Research Fellow with the Department of Science and Technology-Science and Engineering Research Board (DST-SERB), Government of India, New Delhi, India. He was a Postdoctoral Research Fellow with the Research Center for Wind Energy Systems, Kunsan National University, Gunsan, South Korea, from 2017 to 2018. He was a Postdoctoral Research Fellow with the Department of Mathematical Sciences, Shibaura Institute of Technology, Saitama, Japan, from 2018 to 2020. He was a Postdoctoral Research Fellow with the Computational Intelligence Laboratory, Toyota Technological Institute, Japan. He is currently an Associate Professor with Eastern Michigan Joint College of Engineering, Beibu Gulf University, Qinzhou, China. He has authored and co-authored more than 100 research papers in various SCI journals. His research interests include deep learning, natural language processing, complex dynamical networks, and cryptography. He serves as a reviewer for various SCI journals.

MOHAMMED H. ALSHARIF received the M.Sc.Eng. and Ph.D. degrees in electrical engineering from the National University of Malaysia, in 2012 and 2015, respectively. He is currently an Associate Professor with the Department of Electrical Engineering, Sejong University, South Korea. He has authored over 160 articles published in prestigious SCI/E journals in electrical and electronics/communications engineering, including IEEE, Elsevier, Springer, and MDPI. His work has garnered more than 7 212 citations, with an H-index of more than 43 and an I-10 index of more than 114. His research interests include wireless communications, network information theory, the Internet of Things (IoT), and cybersecurity. Additionally, he served as a guest editor for several special issues. For five consecutive years (2020–2024), he was recognized as one of the top 2% scientists globally in Stanford University's report.

MUN-KYEOM KIM received the Ph.D. degree from the School of Electrical and Computer Engineering, Seoul National University. He is currently a Professor with the School of Energy System Engineering, Chung-Ang University, Seoul, South Korea. His research interests include the operation techniques in hybrid AC/DC power systems, AI-based smart power networks, big data-based demand response, real-time market design, and multi-agent-based smart city intelligence.